CHAPTER 9

Spine Imaging

Patrick D. Barnes

The central nervous system (CNS) includes the skull, brain, spine, and spinal cord. The head and neck region includes the face, eye and orbit, nasal cavity and paranasal sinuses, ear and temporal bone, oral cavity, jaw, and neck. Modalities used for the imaging of the pediatric CNS and head and neck region include plain film/computerized radiography (PF/CR), ultrasonography (US), computed tomography (CT) or multidetector CT (MDCT), magnetic resonance imaging (MRI), radionuclide imaging (RI), catheter angiography, and cerebrospinal fluid (CSF) imaging (e.g., CT myelography). Imaging modalities may be classified as structural or functional. Structural imaging modalities provide spatial resolution primarily on the basis of anatomic or morphologic data (e.g., CT). Functional imaging modalities (including molecular imaging) provide spatial resolution on the basis of physiologic, metabolic, or biologic data or markers (e.g., positron emission tomography [PET]). Some modalities may actually be regarded as providing both structural and functional information (e.g., MRI, PET-CT). The technical and procedural descriptions for angiography, myelography, and other invasive and interventional modalities are detailed in other texts. In this presentation, guidelines for their utilization are presented by region and modality.

SPINE IMAGING GUIDELINES

Plain Films/Computerized Radiography

PF/CR is commonly performed for trauma, torticollis, scoliosis, and suspected dysraphism. Occasionally, it may be the initial screening technique for evaluation of pain or any other symptoms or signs relating to the spine. Frontal and/or lateral views may be obtained initially. Oblique views are rarely needed. For scoliosis, erect posterior-anterior frontal and/or lateral views (with breast shielding) are usually obtained. Bending films may also assist in this evaluation. Flexion-extension lateral PF/CR or fluoroscopy, obtained with cooperation of the patient or supervision by a physician, may be helpful in evaluating potential instability (e.g., in craniocervical anomalies). These are x-ray–based techniques that are being increasingly displaced, or replaced, by the other modalities, especially MRI. Such techniques are best used in a limited and selective manner to minimize radiation exposure using the "as low as reasonably achievable" (ALARA) principle.

Ultrasonography

US is often helpful for evaluating the spinal contents in the fetus, newborn, and young infant. Imaging is performed, both static and real-time, with high-resolution, linear-array transducers (5- or 7-MHz) in the sagittal and axial planes. The patient is scanned in the prone position, but sometimes in the supine position, especially if cord tethering is a clinical consideration. Real-time visualization allows dynamic evaluation of the spinal cord and cauda equina nerve roots (i.e., pulsations). Scanning may be facilitated by spinal flexion to widen the interspinous acoustic window.

Computed Tomography

CT imaging of the spine has long replaced conventional tomography and is most often performed without the use of intravenous (IV) or intrathecal CSF administration of contrast material for enhancement. MDCT is replacing PF/CR and becoming the standard for the emergency evaluation of spine trauma, especially for the cervical spine. This evaluation includes high-resolution axial images with sagittal and coronal reformatting using bone and soft tissue algorithms. CT continues to be the choice for assessment of localized bony abnormalities, or a calcified component, of the spinal canal, foramina, neural arches, and articular structures, particularly when the level is precisely defined clinically or by plain film, single-photon emission CT (SPECT), or MRI (e.g., diastematomyelia, spondylolysis, spinal stenosis, spondylitis, bone tumor—i.e., osteoid osteoma, aneurysmal bone cyst). Axial sections with two-dimensional (2D) reformatting (coronal, sagittal, oblique), and/or three-dimensional (3D) reconstructions are often important in the preoperative evaluation of spine trauma, craniocervical anomalies, and congenital scoliosis as well as for the postoperative assessment of instrumentation and fusion. CT may also be obtained (with patient cooperation or physician supervision) with the spine in flexion and extension or with right and left head turning, to evaluate for translational craniocervical instability or rotatory atlantoaxial (AA) instability or fixation, respectively. CT-myelography is rarely needed except when MRI is contraindicated or spinal instrumentation does not allow adequate MRI quality. It may also assist in the more precise delineation of nerve root or other intradural lesions (e.g., cysts). A water-soluble, low-osmolar, non-ionic contrast material specifically approved for myelography is used because of its low toxicity and infrequent side effects. The technical and procedural descriptions for this and other invasive CSF imaging methods are described in detail in other texts. Again, these techniques are best used in a limited and selective manner and using ALARA guidelines to minimize radiation exposure.

Radionuclide Imaging (RI)

Bone scintigraphy, especially SPECT, is frequently helpful for evaluating children with lesions of the spinal column. Back pain, scoliosis, hip or knee pain, limp, and fever of uncertain source may be due to spondylitis, trauma, or tumor. The initial diagnosis may be suggested by bone RI findings. PET (including PET-CT) is also used in the assessment of treatment response or tumor progression in childhood neoplasia.

Magnetic Resonance Imaging

MRI using a phased-array (e.g., multichannel) surface coil system for spinal imaging, or a combined volume head coil and spine surface coil system for craniospinal imaging, has become the ideal modality for definitive evaluation of the spinal neuraxis in children with myelodysplasias (e.g., tethered cord) or myelopathy (e.g., hydrosyringomyelia). Although MRI has improved in its ability to evaluate disk and cortical bony disease, its main advantage over CT for imaging of the extradural structures is in inflammatory and neoplastic involvement of the spinal marrow and paraspinal soft tissues (e.g., osteomyelitis, neuroblastoma, plexiform neurofibroma), especially using fat suppression techniques. The addition of the contrast agent gadolinium to the fat suppression techniques further enhances the ability of MRI to evaluate inflammation and tumor, whether intramedullary, intradural, or extradural. Although MRI is the procedure of choice for initial

evaluation of suspected vascular lesions (e.g., arteriovascular malformation), angiography is the definitive procedure, particularly when interventional therapy is being considered.

In general, screening spine MRI begins with sagittal T1-weighted and T2-weighted images plus axial T2-weighted images of the entire spine (as one or more series) from the posterior fossa through the coccyx. Axial T1- and T2-weighted images are obtained from the conus medullaris through the dural sac to confirm the conus level and to evaluate for filar thickening, extent of a dermal sinus, and a tethering mass (e.g., lipoma, dermoid-epidermoid). Axial images are imperative for surgical planning (e.g., lipomyelomeningocele). Coronal T2-weighted images assist in evaluating for spinal column anomalies (e.g., hemivertebra in congenital scoliosis), split-cord malformations (e.g., diastematomyelia), and renal anomalies. In cases of diastematomyelia, axial T2-weighted images through the split cord are necessary to demonstrate or rule out a tethering septum. Sagittal T2-weighted images are important for evaluating hydrosyringomyelia and Chiari I malformation along with axial T2-weighted images. Gadolinium-enhanced T1-weighted imaging is also necessary to assess for tumor as a cause of cord expansion or hydrosyringomyelia. Craniospinal imaging is often done to evaluate patients for the sequelae of repaired myelomeningocele and Chiari II malformation, including ventricular size, possible fourth ventricular isolation, and hydrosyringomyelia, as well as for sequelae at the original repair site (e.g., scarring, dermoid-epidermoid). Sagittal and axial T2-weighted MRI may also be done in flexion and extension (with patient cooperation or physician supervision) to assess craniocervical instability or fixation (e.g., craniocervical anomalies).

For evaluation of extradural traumatic, inflammatory, or neoplastic processes (e.g., ligamentous injury, disk herniation, osteomyelitis, sarcoma), sagittal T1-weighted images are performed, followed by sagittal fat-suppression T2-weighted images or short TI inversion recovery (STIR) images. Axial T2-weighted images are also important. Additional gadolinium-enhanced sagittal and axial fat-suppression T1-weighted images are necessary for evaluating neoplastic and inflammatory processes, as well as for assessing disk protrusion after surgery. These techniques allow for the complete assessment of marrow, bony, and paraspinal soft tissue involvement and extent as well as for cord, cauda equina, or nerve root compression. Diffusion-weighted MRI has been used to assist in the differentiation of traumatic vs. pathologic spinal fracture. Gadolinium enhancement is also necessary in the assessment of intramedullary tumors (e.g., astrocytoma, ependymoma, ganglioglioma), and intradural tumors (e.g., neurofibroma, schwannoma, ependymoma), and for neoplastic seeding (e.g., medulloblastoma, germ cell tumors).

Sagittal T2-weighted or STIR imaging, along with axial T2-weighted imaging, is done to evaluate for intramedullary inflammation or degeneration, including the assessment of cord atrophy. Gadolinium-enhanced imaging may also be helpful. A combination of sagittal and coronal T1- and T2-weighted imaging plus axial T2-weighted imaging is performed for screening of patients with suspected spinal vascular malformation. T2* gradient echo imaging may further detect hemorrhage. Gadolinium-enhanced imaging is occasionally needed in such patients, particularly to rule out other abnormalities. Gadolinium-enhanced MR angiography may be useful, but angiography is the "gold standard," especially for surgical planning and for interventional neuroradiologic guidance.

NORMAL DEVELOPMENT OF THE SPINAL NEURAXIS AND SPINAL COLUMN

The *spinal neuraxis* (spinal cord and nerve roots) develops through the process of *neurulation* (neural tube closure). The notochord induces the formation of the neural plate, which is neural ectoderm continuous with cutaneous ectoderm. The neural plate is the origin of both the neural tube, from which the CNS forms, and the neural crest, from which the peripheral nervous system is derived. Closure of the neural groove forms the brain and mid- to upper spinal cord by the fourth week, including separation from the adjacent ectoderm, endoderm (i.e., neurenteric canal), and mesoderm. The dorsal root ganglia, cranial and spinal nerves, and sympathetic chain form from the neural crest. The distal conus medullaris, associated nerve roots, and filum terminale form as a result of canalization and retrogressive differentiation of the caudal neural tube (caudal cell mass origin). Rapid longitudinal growth of the spinal column occurs so that the conus is usually at or above the mid-L2 vertebral body level before 1 year postnatal age.

The *spinal column* forms as the result of membrane development (i.e., formation phase) followed by chondrification and then ossification. The notochord separates from the primitive gut and dorsal neural tube (i.e., neurenteric canal) during the fourth week of gestation. This mesenchyme subsequently forms a series of somites, or segments (i.e., segmentation phase), which become the spinal column and paraspinal tissues. Remnants of the notochord persist as the nucleus pulposus of the intervertebral disk. The components of the craniocervical junction, which arise from the primordial occipital and cervical sclerotomes, consist of the occipital bone, atlas (C1), axis (C2), and associated ligaments. More detailed descriptions of CNS embryology and development are covered in other texts. Knowledge of the normal spine and its variations of normal is important for proper image interpretation of findings of PF/CR, US, CT, and MRI. This subject is also covered in greater detail elsewhere.

DEVELOPMENTAL ABNORMALITIES

Dysraphic Myelodysplasias

The most common group of spinal neuraxis and column malformations, dysraphic myelodysplasias result from disorders of spinal neural tube closure (Box 9-1). *Dysraphism* refers to defective midline closure of neural, bony, and other mesenchymal tissues. *Spina bifida "aperta"* refers to the direct exposure of neural tissue through a dorsal bony spinal and cutaneous defect. Within this subcategory are myelocele, myelomeningocele, hydromyelia, Chiari II malformation, hemimyelocele, myeloschisis, and craniooschisis. In "occult" spinal dysraphism, the myelodysplasia lies deep to intact skin. This subcategory includes dermal sinus, lipomyelomeningocele, tight filum terminale, meningocele, myelocystocele, diastematomyelia, neurenteric cyst, the split notochord syndrome, and developmental tumors such as spinal lipomas. In both subcategories, cutaneous stigmata are common and include the exteriorized placode associated with the myelocele and myelomeningocele, as well as skin-covered lesions such as subcutaneous lipoma, hairy patch (hypertrichosis), nevus, hemangioma, and dermal sinus. Plain film findings may show formation or segmentation anomalies, congenital scoliosis or kyphosis, canal widening, or spinolaminar defects. CT is helpful for preoperative definition of the bony spinal anomalies. US is a

Box 9-1. **Dysraphic Myelodysplasias**

Myelocele and myelomeningocele
Lipomyelocele and lipomyelomeningocele
Dermal sinus
Tethered cord syndrome
Myelocystocele
Meningocele
Split notochord syndrome
Neurenteric cyst
Diastematomyelia
Caudal dysplasias
Developmental tumors

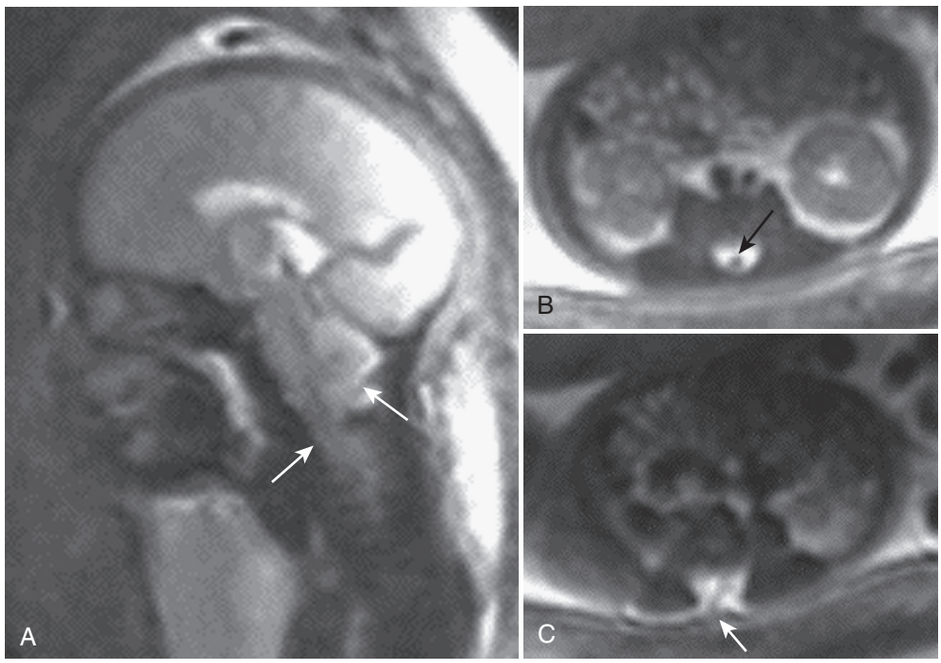

FIGURE 9-1. Fetal T2-weighted MR images. **A,** Chiari II malformation (*arrows*) on sagittal image. **B,** Lumbosacral myelocele with low-placed spinal cord (*arrow*) on axial image. **C,** Dysraphic defect plus placode (*arrow*) on axial image.

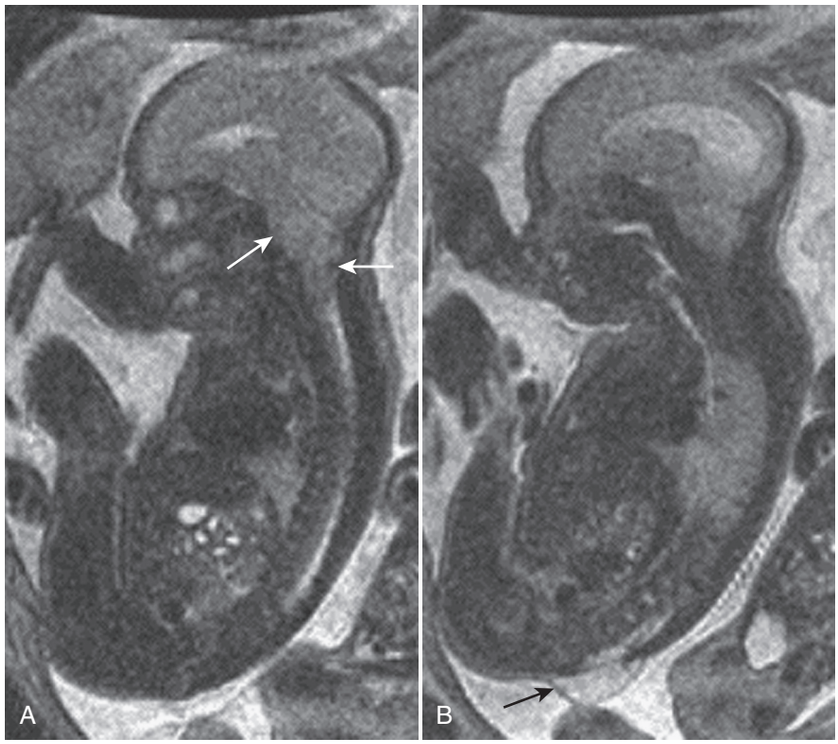

FIGURE 9-2. Chiari II malformation (*arrows* in **A**) and lumbosacral myelomeningocele (*arrow* in **B**) on sagittal T2-weighted fetal MR images.

useful screening modality for the fetus and young infant and is also used for intraoperative surgical guidance. MRI is the definitive modality for diagnosis, surgical planning, and follow-up.

Myelocele and Myelomeningocele

Both myelocele and myelomeningocele are the result of nondisjunction of the cutaneous ectoderm from the neural ectoderm and failure of neural tube closure. The nonneurulated cord or placode is exposed through a dural, bony, and cutaneous defect (i.e., myelocele; Fig. 9-1). The dorsal and ventral nerve roots exit from the ventral surface of the placode. With associated dorsal protrusion of the ventral subarachnoid space, the myelodysplasia is termed a *myelomeningocele* (Fig. 9-2). These defects commonly occur at the lumbar or sacral level. Occasionally there is an associated diastematomyelia (hemimyelomeningocele) or dermal sinus.

These defects are surgically closed shortly after birth. Hydrocephalus is often present; if so, shunting is established early. Subsequently, patients who have undergone such procedures may

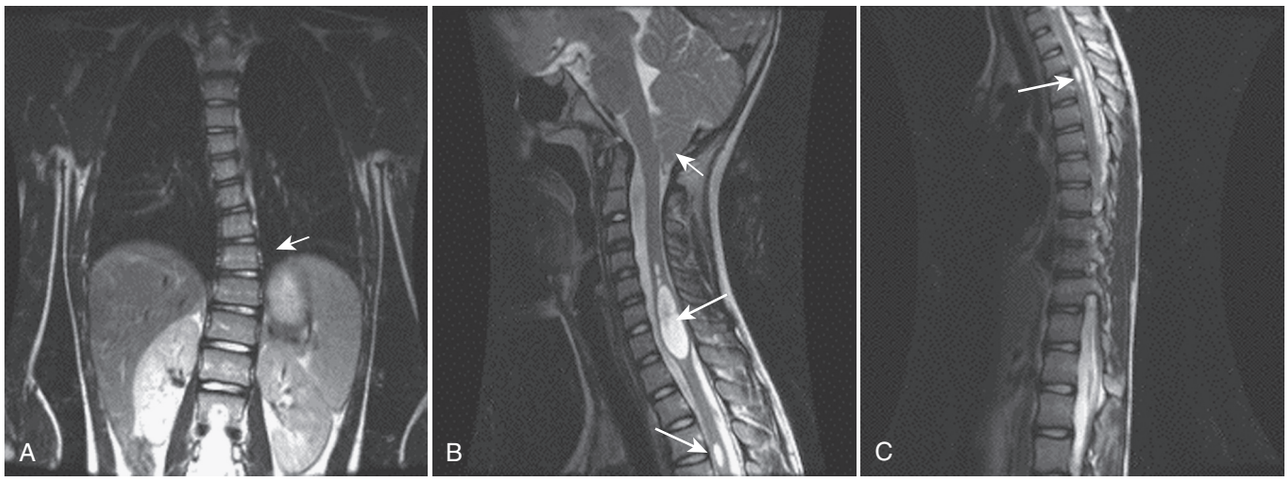

FIGURE 9-3. Chiari I malformation and cervicothoracic hydrosyringomyelia on T2-weighted MRI. **A,** Coronal image showing left thoracic curve (*arrow*). **B** and **C,** Sagittal images showing low cerebellar tonsils (*short arrow* in **B**), and cyst-like cord expansions (*long arrows* in **B** and **C**).

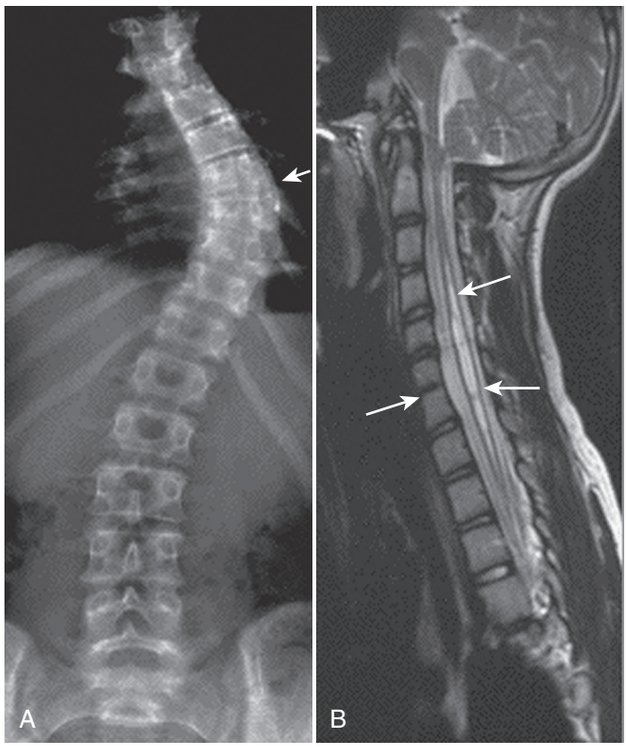

FIGURE 9-4. Klippel-Feil anomaly with hydrosyringomyelia. **A,** Frontal plain film/computerized radiograph shows left thoracic lateral curve (*arrow*). **B,** Sagittal T2-weighted MR image shows C6 to C7 bony fusion anomaly (*anterior arrow*), small C1 canal, and C3 to T2 septated cord expansion (*posterior arrows*).

undergo neuroimaging for any change in neurologic status that may be related to the Chiari II malformation (see Figs. 9-1 and 9-2), to associated anomalies, or to the sequelae of surgical closure or shunted hydrocephalus. Associated conditions or sequelae include hydrocephalus, shunt malfunction, encystment of the fourth ventricle, hydrosyringomyelia, brainstem compression or dysfunction, cervical cord compression or constriction, hemimyelocele/hemimyelomeningocele, lipoma, dermoid-epidermoid, arachnoid cyst, scarring or retethering at the operative site, dural sac stenosis, progressive scoliosis, and cord ischemia or infarction.

Hydrosyringomyelia

Hydromyelia refers to dilatation of the central canal of the spinal cord; *syringomyelia* refers to a spinal cord cavity. Since one may be indistinguishable from the other, or the two conditions may coexist, the term *hydrosyringomyelia* is often used. This condition is most commonly associated with the Chiari malformations (e.g., Chiari I, II), spinal dysraphism, and craniocervical anomalies. MRI may demonstrate focal, segmental, or total involvement of the spinal cord (Figs. 9-3 to 9-6). Intramedullary CSF intensities are present, and the cord may be enlarged. Sacculations or septations may be present. Syrinx or cyst may also occur with trauma, infection, tumors, or arachnoiditis.

Lipomyelocele and Lipomyelomeningocele

Lipomyelocele and lipomyelomeningocele are the most common of the occult myelodysplasias. Like the myelocele and myelomeningocele, they result from faulty disjunction, but the skin is intact and there is an associated lipoma. Patients with these defects may be asymptomatic, may present with a subcutaneous mass, or may have motor or sensory loss, bladder dysfunction, or orthopedic deformities of the lower extremities. The lipoma often extends caudally, dorsally, or ventrally from the incompletely fused cord (e.g., presacral) through a dural and bony defect and is continuous with the subcutaneous fat. The spinal canal is often enlarged. Spina bifida or formation-segmentation anomalies may be present. For surgical planning, MRI demonstrates the relationships of the lipoma, which is hyperintense on T1-weighted imaging (T1-hyperintense), with the neural elements (Figs. 9-5 to 9-7). There may be an associated thickened filum or filar lipoma (Fig. 9-7).

Dermal Sinuses

Dermal sinuses are epithelial tracts, stalks, or fistulae that extend from the skin surface into the deeper tissues. They result from incomplete dysjunction of the neuroectoderm from the cutaneous ectoderm during neurulation and may occur in the lumbosacral, cervicooccipital, or thoracic region. There is often a midline dimple or ostium with an associated hairy nevus, vascular anomaly, or hyperpigmentation. The sinus often extends into the deeper tissues and enters the spinal canal. It may even extend to the dura or penetrate the dura and terminate in the subarachnoid space, the filum, or the conus medullaris. There may be an

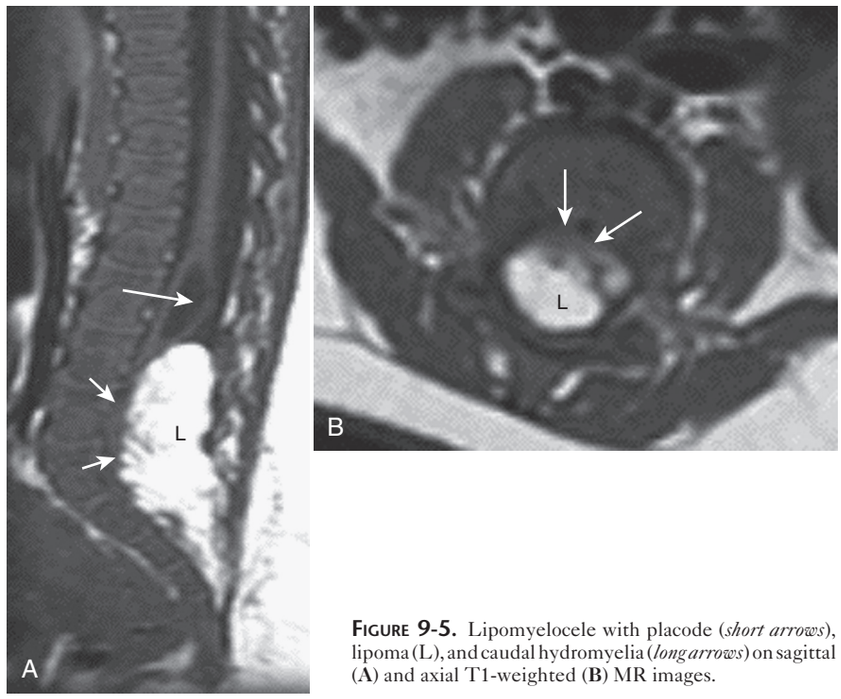

FIGURE 9-5. Lipomyelocele with placode (*short arrows*), lipoma (L), and caudal hydromyelia (*long arrows*) on sagittal (**A**) and axial T1-weighted (**B**) MR images.

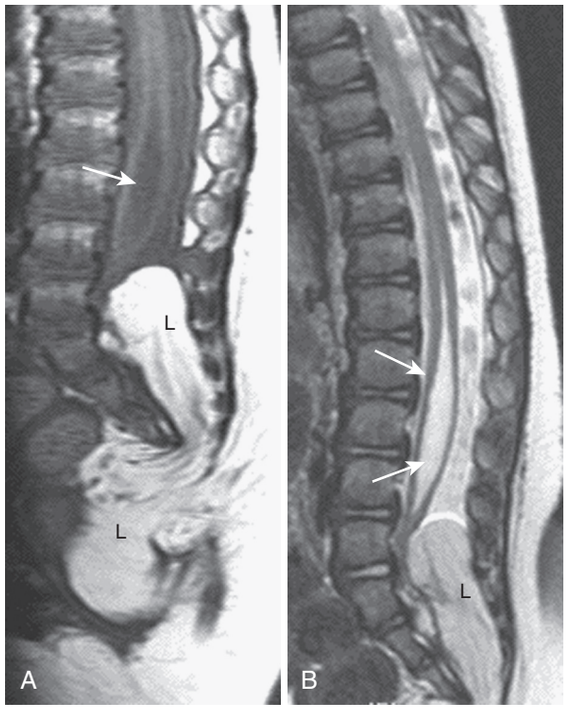

FIGURE 9-6. Lumbosacral lipomyelocele with caudal and presacral lipomas (L) and hydrosyringomyelia (*arrows*) on sagittal T1-weighted (**A**) and T2-weighted (**B**) MR images.

associated dermoid-epidermoid or lipoma (Figs. 9-8 and 9-9). Affected patients may present with abscess or meningitis. On MRI the dermal sinus usually appears as a relative hypointensity. Gadolinium may be helpful, especially when infection is present (Fig. 9-10).

The Tethered Cord Syndrome

Also known as "tight filum terminale syndrome," *tethered cord syndrome* refers to low position of the conus medullaris (below the level of mid-L2) associated with a short and thickened filum terminale. The filar thickening (usually greater than 2 mm) is usually fibrous, fatty, or cystic, and may be associated with other dysraphic myelodysplasias, including lipomyelomeningocele and diastematomyelia. The thickened filum may also terminate in a lipoma or dermoid-epidermoid. The filar abnormality is usually best demonstrated on axial T1-weighted and T2-weighted MRI (Fig. 9-11; see Fig. 9-7).

Myelocystocele

Myelocystocele is the least common of the occult myelodysplasias associated. This defect usually occurs at the lumbosacral level (rarely at the cervical level) and is often associated with other malformations of caudal cell mass origin (i.e., anorectal and urogenital anomalies—high imperforate anus, cloacal malformation, etc.). The terminal myelocystocele consists of hydromyelia and a dilated terminal ventricle of the conus-placode that is continuous with a dorsal, ependyma-lined cyst within or adjacent to a meningocele. There may be an associated lipoma (i.e., lipomyelocystocele).

Meningoceles

Meningoceles are uncommon, saccular dural protrusions that extend beyond the confines of the spinal canal and contain CSF-filled arachnoid but no cord elements. They may extend dorsally, laterally, or ventrally. Dorsal dysraphic meningoceles may occur at the occipital, cervicooccipital, or lumbosacral level. An anterior meningocele extending through a dysraphic defect may be considered a neurenteric spectrum anomaly. Presacral meningoceles associated with dysraphic defects are often associated with anorectal or urogenital anomalies in the caudal dysplasia spectrum. Meningoceles extending laterally through an intervertebral foramen, or anteriorly through a sacral foramen, may be seen with a mesodermal dysplasia such as neurofibromatosis type 1 (NF-1) or Marfan syndrome (Fig. 9-12).

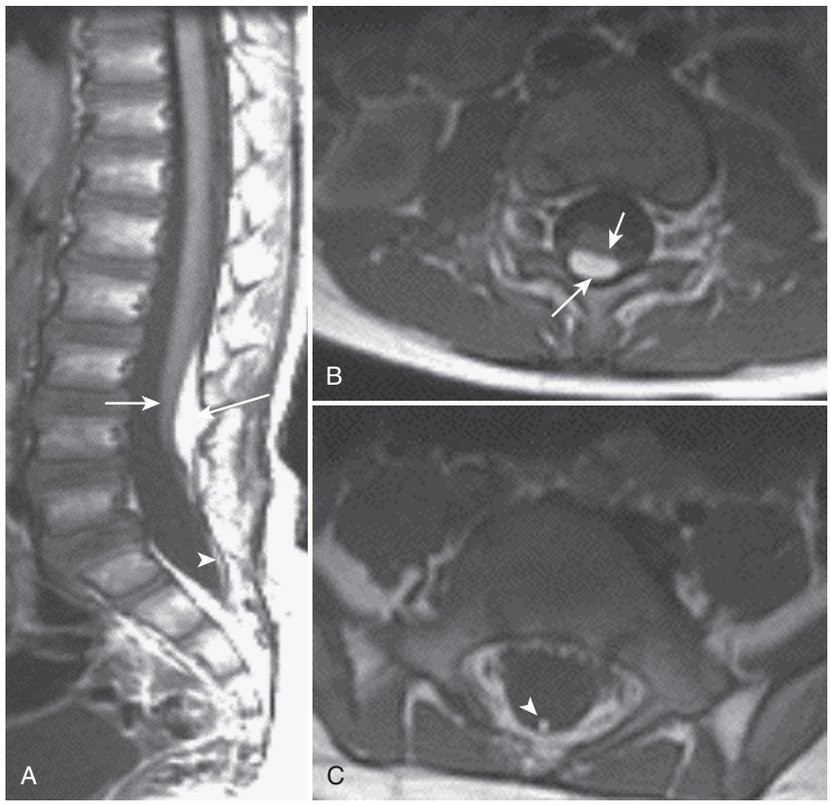

FIGURE 9-7. Sagittal (**A**) and axial (**B** and **C**) T1-weighted MR images showing tethered cord with low conus (*short arrows* in **A** and **B**), dorsal lipoma (*long arrows* in **A** and **B**), and filar lipoma (*arrowheads* in **A** and **C**).

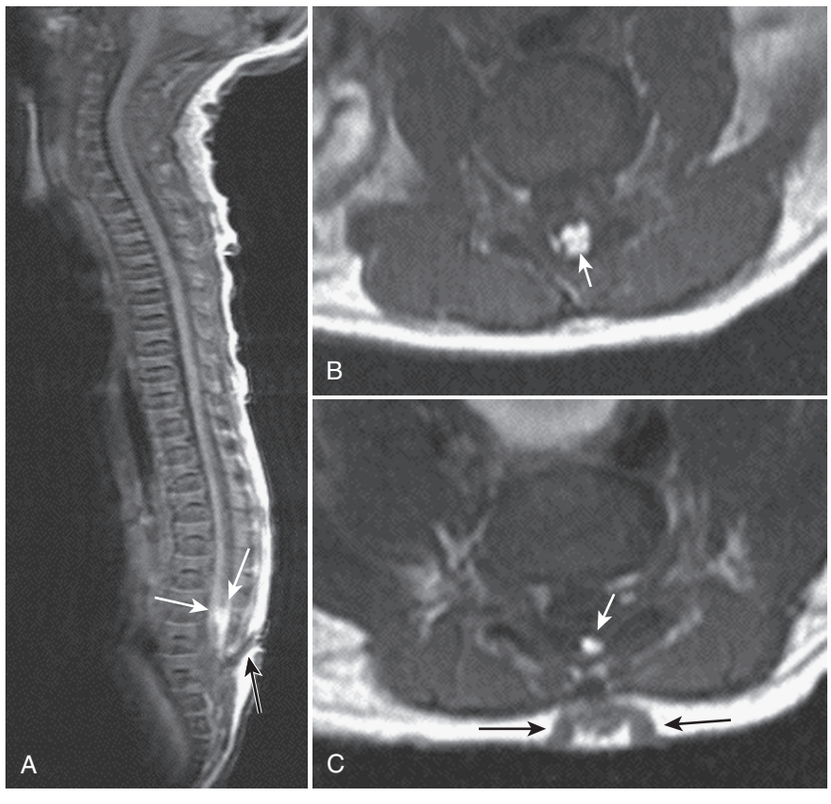

FIGURE 9-8. Sagittal (**A**) and axial (**B** and **C**) T1-weighted MR images showing lumbosacral dermal sinuses (*black arrows* on **A** and **C**) with tethered cord (*white arrows* in **A**) and lipoma (*white arrows* in **B** and **C**) in a newborn.

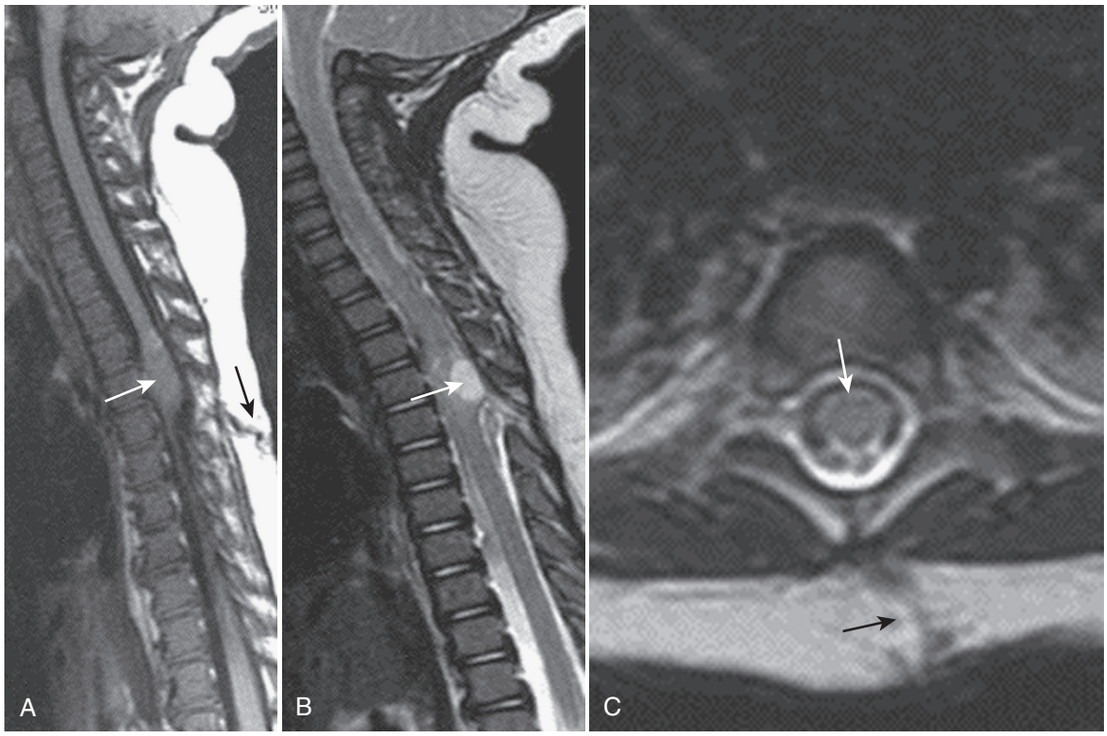

FIGURE 9-9. Thoracic dermal sinus (*black arrows*) and dermoid cyst (*white arrows*) on sagittal T1-weighted (**A**), sagittal T2-weighted (**B**), and axial T1-weighted (**C**) MR images.

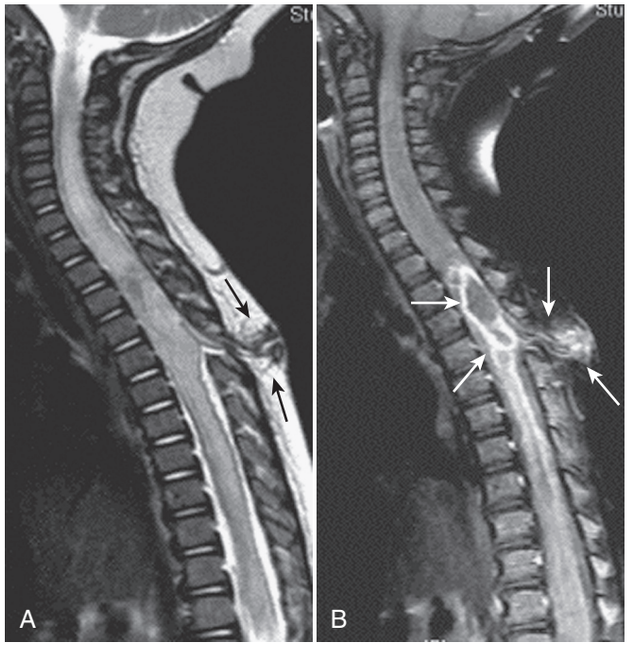

FIGURE 9-10. Thoracic dermal sinus (*posterior black and white arrows* in **A**, and **B**) and cyst with enhancing abscess (*anterior white arrows* in **B**) with cord edema on sagittal T2-weighted (**A**) and gadolinium-enhanced T1-weighted (**B**) MR images.

The Split Notochord Syndrome

Split notochord syndrome refers to a rare spectrum of malformations related to the incomplete separation of the endoderm and ectoderm during the formation of the notochord (i.e., complete or partial failure of obliteration of the primitive neurenteric canal). The spectrum includes dorsal enteric fistula, dorsal enteric sinus, dorsal enteric enterogenous cysts, and dorsal enteric diverticula.

Neurenteric Cyst

Neurenteric cyst is also an anomaly of the neurenteric spectrum. Such cysts usually arise in the lower cervical or thoracic region. Associated formational vertebral anomalies include butterfly vertebra, hemivertebra, and block vertebra. A classic presentation is that of a posterior mediastinal mass associated with vertebral anomalies. The intraspinal lesions are usually intradural and extramedullary in location. However, they may occur in a prevertebral or dorsal location or may involve multiple compartments. The cyst may be lined by gut or respiratory epithelium and may have serous contents similar to CSF or may contain mucoid secretions and appear T1-hyperintense.

Diastematomyelia

The most common anomaly of the neurenteric or split notochord spectrum is diastematomyelia. It consists of sagittal clefting of the cord into symmetric or asymmetric hemicords. In some cases, the split is traversed by a septum and each hemicord has its own pial, arachnoid, and dural coverings (Fig. 9-13). In other cases, the hemicords are contained within a single dural sac and there is no septum (Fig. 9-14). The septum may be bony, cartilaginous, fibrous, or may be composed of vascular elements or neuroglial tissue. The hemicords often rejoin above and below the cleft. This malformation occurs most commonly in the lumbar or thoracolumbar region and is often associated with cutaneous stigmata. PF/CR or CT may show spina bifida, intersegmental laminar fusion, anomalies of the vertebral bodies, and kyphoscoliosis. For septal definition, axial T2-weighted MRI, CT, or myelographic CT is necessary. Associated anomalies include thickened filum, developmental tumor (e.g., lipoma, dermoid-epidermoid), hydromyelia, and tethering bands (meningocele manqué).

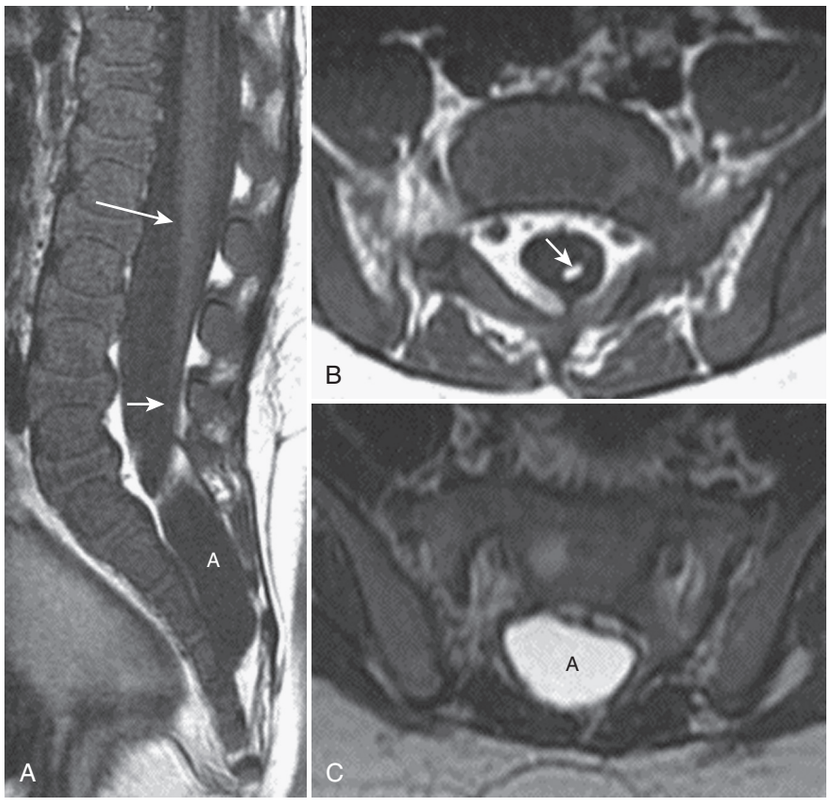

FIGURE 9-11. Tethered cord (*long arrow*), thick filum and lipoma (*short arrows*), and sacral extradural arachnoid cyst (A) on sagittal T1-weighted (**A**), axial T1-weighted (**B**), and axial T2-weighted (**C**) MR images.

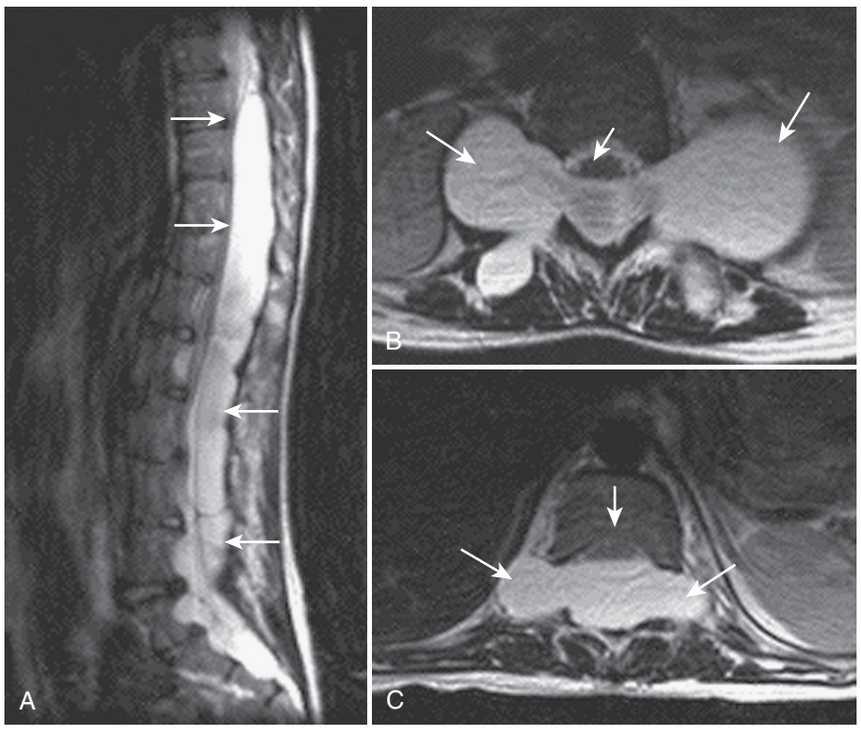

FIGURE 9-12. Sagittal (**A**) and axial (**B** and **C**) T2-weighted MR images showing dural ectasia and intradural arachnoid cysts (*arrows* in **A**) with scoliosis, cord flattening (*short arrows* in **B** and **C**), and transforaminal meningoceles (*long arrows* in **B** and **C**).

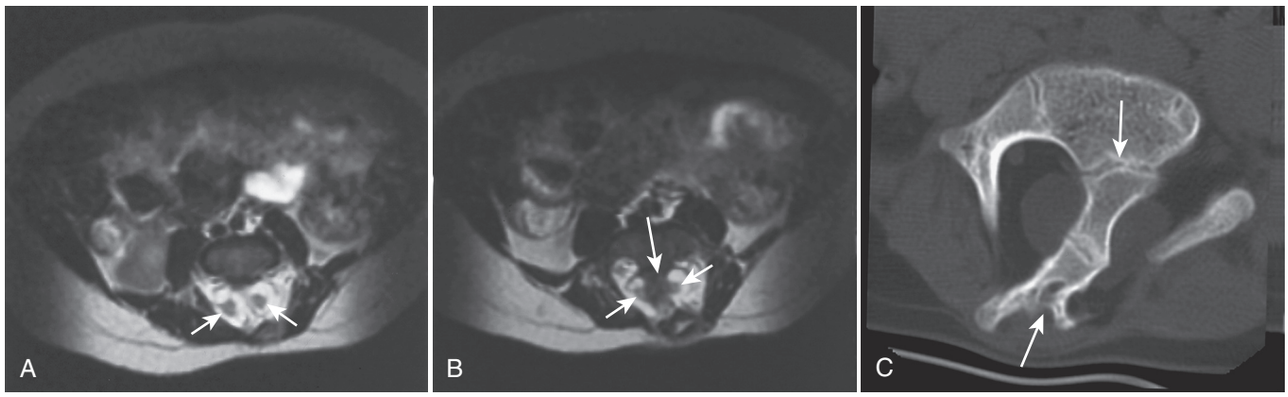

FIGURE 9-13. Lumbar diastematomyelia and split cord with two hemicords (*short arrows* in **A** and **B**), two dural sacs, and a bony septum (*long arrows* in **B** and **C**) on axial T2-weighted MR images (**A** and **B**) and an axial CT scan (**C**).

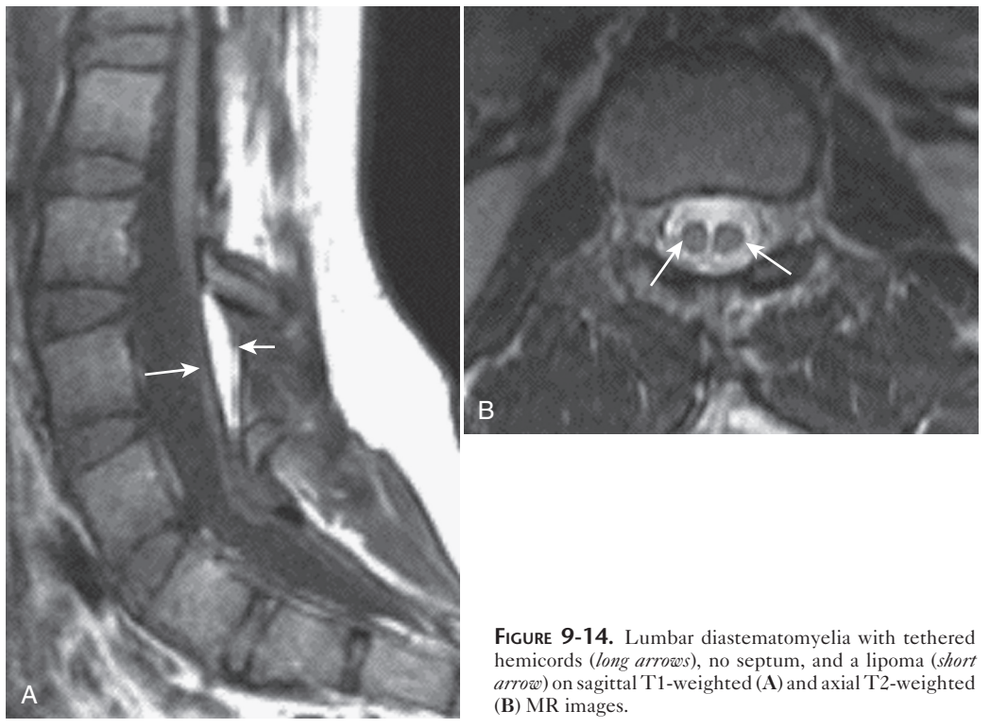

FIGURE 9-14. Lumbar diastematomyelia with tethered hemicords (*long arrows*), no septum, and a lipoma (*short arrow*) on sagittal T1-weighted (**A**) and axial T2-weighted (**B**) MR images.

The Caudal Dysplasias

The caudal dysplasias are a spectrum of malformations of caudal cell mass origin that include lumbosacral, anorectal, urogenital, and lower limb anomalies. In children with high imperforate anus, cloacal malformation, or cloacal exstrophy, there is a high prevalence of dysraphic myelodysplasia. The spinal anomalies range from dysraphism to partial to total sacral or lumbosacral agenesis. MRI may demonstrate a high-positioned and blunted or wedge-shaped conus termination (Fig. 9-15). There may be spinal canal or dural sac stenosis. Other anomalies are presacral meningocele or lipoma (see Fig. 9-6), cord tethering with filar thickening or developmental tumor, lipomyelomeningocele, and myelocystocele. The *caudal regression syndrome* is composed of lower extremity fusion (sirenomelia), lumbosacral agenesis, anal atresia, abnormal genitalia, exstrophy of the bladder, renal aplasia, and pulmonary hypoplasia. This may be associated with Potter syndrome or may be seen in infants of diabetic mothers.

Developmental Tumors

Developmental tumors of the spinal neuraxis include lipoma, dermoid-epidermoid, teratoma, arachnoid cyst, neurenteric cyst, and hamartoma.

Lipomas are the most common. They may arise as intradural lipomas, lipomyeloceles, lipomyelomeningoceles, or filar lipomas (see Figs. 9-5 to 9-8, 9-11, 9-14). Intradural lipomas usually occur as dorsal cervical or thoracic subpial masses. MRI of a lipoma demonstrates a lobulated T1-hyperintense mass adherent to or occupying a cord cleft.

Dermoids are tumors of ectodermal origin that contain elements of the dermis and epidermis (i.e., skin, hair, sweat and sebaceous glands, squamous epithelium). *Epidermoids* are composed of epidermal elements only. Both of these tumors may contain the products of squamous epithelial turnover (i.e., keratin and cholesterol). They arise most commonly from congenital rests but may also occur as implants after surgery or spinal puncture. Dermoids and epidermoids are often extramedullary but may arise within

the medulla. There may be associated dermal sinus, cord tethering, abscess, or suppurative or chemical meningitis. On MRI they may be T1-isointense to hypointense and T2-hyperintense. Occasionally, there is fatlike hyperintensity or calcification (see Fig. 9-9). Enhancement may be evident because of inflammation (see Fig. 9-10).

Teratomas are neoplasms containing elements of all three germ layers. A teratoma arising in the sacrococcygeal region is common in childhood and manifests as an external perineal or gluteal mass, a pelvic mass, or a presacral mass. Two thirds are mature teratomas, and one third are immature or anaplastic teratomas. They are often lobulated and heterogeneous with solid, cystic, and calcific components. There may be associated sacral bony erosion. There is a familial form with an autosomal dominant inheritance that is associated with sacrococcygeal defects, vesicoureteral reflux, anorectal stenosis, and cutaneous stigmata (Currarino syndrome). These tumors often have heterogeneous MRI signal characteristics. Teratomas of the spinal canal are rare, are often benign, and usually occur as intramedullary or extramedullary masses at the thoracolumbar level.

Arachnoid cysts are categorized as primary or secondary (e.g., postinflammatory). Primary cysts may be intradural or extradural in location, and secondary cysts are usually intradural and associated with arachnoiditis. Although these cysts usually occur in the thoracic or lumbar region, they may be seen at any level. There may be scoliosis and spinal canal widening. MRI demonstrates a CSF-intensity cyst that displaces the cord, nerve roots, or epidural fat (see Figs. 9-11 and 9-12).

Hamartomas are masses that contain tissues of neuroectodermal or mesodermal origin—neuroglial and meningeal tissue, bone, fat, cartilage, or muscle. They are solid or cystic subcutaneous masses that occur in the mid-thoracic, thoracolumbar, or lumbar region and are often associated with cutaneous angiomas. Spina bifida and spinal canal widening are often seen with hamartomas.

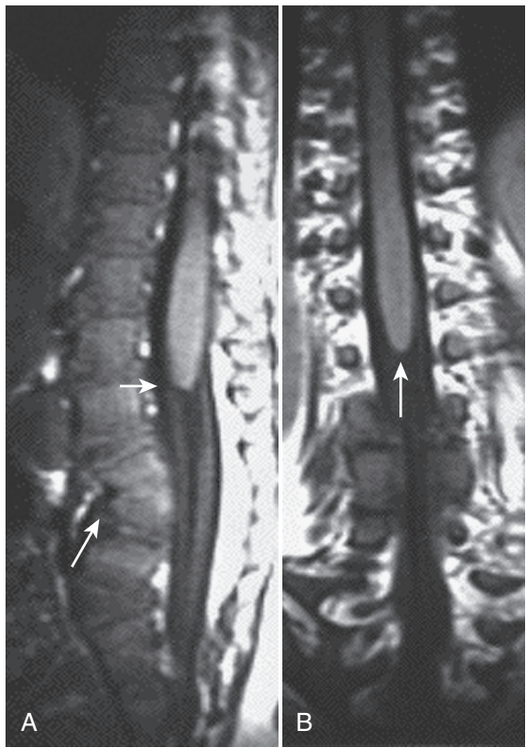

Figure 9-15. Caudal dysplasia with high imperforate anus, congenital lumbar kyphosis (*long arrow*s), and dysplastic/hypoplastic conus medullaris (*short arrow*) on sagittal (**A**) and coronal (**B**) T1-weighted MR images.

Spondylodysplasias

Spondylodysplasia refers to any developmental abnormality of the bony spinal column (Box 9-2). This category includes idiopathic scoliosis, congenital scoliosis and kyphosis, Scheuermann disease, and the skeletal dysplasias (e.g., NF-1, mucopolysaccharidoses, spondyloepiphyseal dysplasia, achondroplasia, Down syndrome). Spinal curvature abnormalities are common in this category. As defined by clinical examination and findings on standing plain films, they include scoliosis (lateral curvature), kyphosis (posterior angulation), and lordosis (increased anterior angulation). In the skeletal dysplasias, a major concern is mechanical compromise of the spinal neuraxis due to progressive canal/foraminal stenosis, kyphoscoliosis, or craniocervical instability. Evaluation usually requires both CT and MRI.

Idiopathic Scoliosis

Idiopathic scoliosis is the most common curvature abnormality in childhood. The adolescent form, which is seen in children older than 10 years, is more common than the infantile or juvenile form. Adolescent idiopathic scoliosis is familial and most commonly seen in females. Characteristically, there is a right convex primary curve of the thoracic, thoracolumbar, or lumbar spine (Fig. 9-16). A rotatory component with pedicle asymmetry is characteristic, and a left convex secondary curve may present. Additional lordosis often occurs with curve progression. Complications of idiopathic scoliosis include curve progression, cardiopulmonary compromise, painful curves, cosmetic deformity, neurologic dysfunction, and degenerative joint disease. Curve progression usually occurs during periods of growth acceleration (e.g., infancy and prepuberty). Treatment may be required and involves bracing or surgical instrumentation and fusion (e.g., Harrington rods).

Atypical clinical or plain film findings in "presumed" idiopathic scoliosis require MRI to evaluate for an underlying abnormality such as hydrosyringomyelia (e.g., Chiari malformation), tumor, cyst, or dysraphic myelodysplasia (see Figs. 9-3, 9-4, 9-12). Atypical clinical features include early onset (prior to age 10 years), rapid curve progression, painful curves in young children, and abnormal neurologic symptoms or signs. Atypical curve patterns include a convex left primary curve, a kyphotic component, vertebral body or neural arch anomaly, pedicle thinning, and spinal canal widening.

Congenital Scoliosis and Kyphosis

Congenital scoliosis and kyphosis result from formation or segmentation anomalies (Fig. 9-17). Failure of formation may result in vertebral aplasia or hypoplasia with wedge vertebra, hemivertebra, or butterfly vertebra. Anomalies of segmentation failure include pedicle fusion bars and block vertebra. Combined anomalies are also common (e.g., block hemivertebra). Associated myelodysplasia occurs in 15% to 20% of cases of scoliosis or kyphosis (e.g., hydrosyringomyelia, diastematomyelia, neurenteric cyst,

Box 9-2. Spondylodysplasias

Idiopathic scoliosis
Congenital scoliosis and kyphosis
Scheuermann/Schmorl disease
Neurofibromatosis
Achondroplasia
Mucopolysaccharidoses
Down syndrome
Spondyloepiphyseal dysplasia
Craniocervical anomalies
Klippel-Feil syndrome
Spinal vascular anomalies

tethered cord) (see Figs. 9-4, 9-13, 9-17). Cardiac and genitourinary anomalies are also common. Other complications of congenital kyphosis are segmental spinal dysgenesis with congenitally dislocated spine, progressive or acute cord injury, cardiopulmonary compromise, and severe cosmetic deformity. Other causes of kyphosis and kyphoscoliosis in childhood are posture, Scheuermann disease, neuromuscular disorder, trauma, inflammation, surgery, radiation therapy, metabolic disorders, chondrodysplasia, arthritis, and tumor. Lordotic curvature abnormalities may be congenital or acquired.

FIGURE 9-16. Idiopathic scoliosis with typical rightward thoracic lateral and rotatory curvature on a frontal plain film/computerized radiograph (obtained with breast shields in place).

Scheuermann Disease

An osteochondrodysplasia, Scheuermann disease is a common cause of juvenile and adolescent thoracic kyphosis. An abnormality of enchondral ossification is associated with degenerative and reactive changes of the vertebral end plates. Often there is multilevel end plate irregularity, disk space narrowing, vertebral body wedging, and Schmorl nodes (Fig. 9-18). The kyphosis commonly occurs in the mid-thoracic spine. There may be progressive wedging with increasing thoracic kyphosis and lumbar lordosis. The less common lumbar form may be acute, painful, and traumatic. Limbus-like vertebral abnormalities are often seen.

Neurofibromatosis Type 1

NF-1 is a common mesodermal dysplasia of childhood (Fig. 9-19). Characteristic anomalies include a short-segment kyphoscoliosis, posterior vertebral body scalloping, vertebral body wedging, apical vertebral rotation, dural ectasia, and meningoceles (e.g., thoracic, presacral). There may also be an associated plexiform neurofibroma and other nerve sheath tumors. Other anomalies are cervical kyphosis, hypoplasia of the spinous process, transverse process, or pedicle, and twisted-ribbon ribs. Dural ectasia and meningocele formation may also be seen with Marfan or Ehlers-Danlos syndrome and in familial cases (see Fig. 9-12).

Achondroplasia

Achondroplasia is one of the osteochondrodysplasias (defective enchondral bone development) resulting in dwarfism. There is craniofacial dysmorphia with skull base constriction, including foramen magnum stenosis, short clivus, and small jugular foramina (Fig. 9-20). Macrocephaly and hydrocephalus (e.g.,

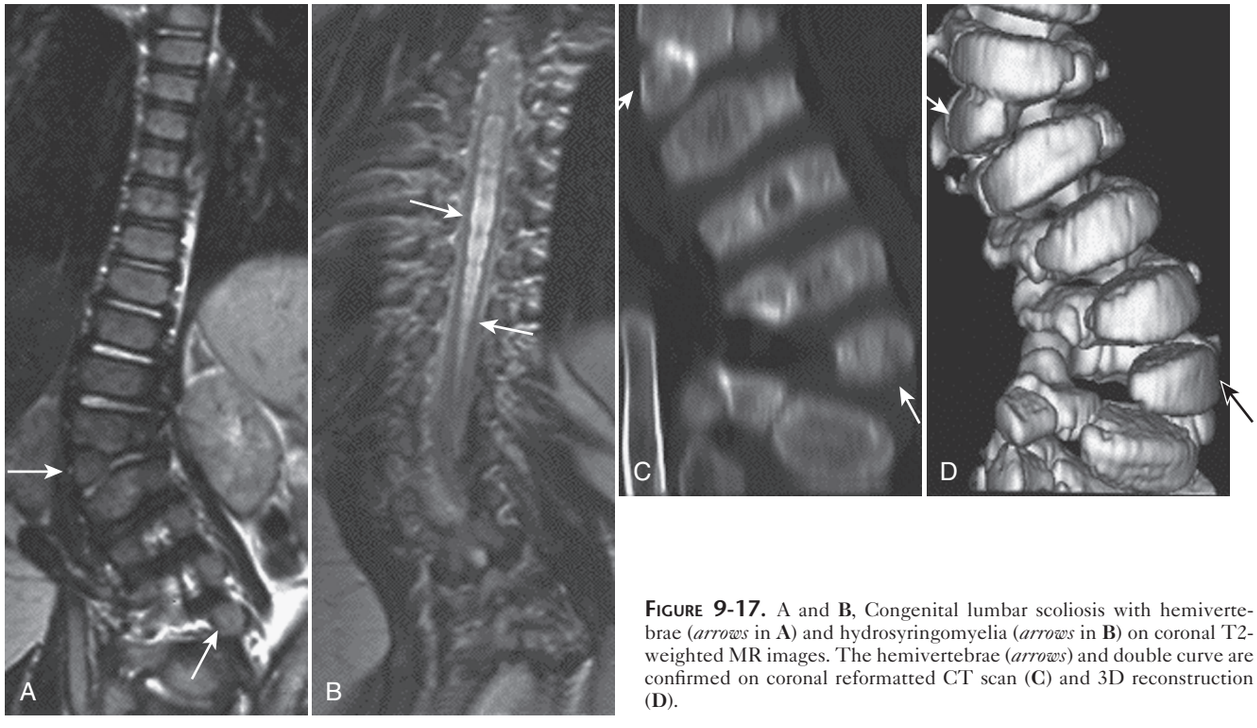

FIGURE 9-17. A and **B**, Congenital lumbar scoliosis with hemivertebrae (*arrows* in **A**) and hydrosyringomyelia (*arrows* in **B**) on coronal T2-weighted MR images. The hemivertebrae (*arrows*) and double curve are confirmed on coronal reformatted CT scan (**C**) and 3D reconstruction (**D**).

impaired venous outflow) occur, and there is enlargement of the subarachnoid spaces and ventricles. Other craniocervical abnormalities include odontoid hypoplasia, atlantoaxial (AA) instability, basilar impression, and occipitalization of the atlas. Scoliosis, kyphosis, or kyphoscoliosis may occur in about one third of patients with achondroplasia. Stenosis of the spinal canal may be cervical, thoracolumbar, lumbar, or may occur diffusely. There is platyspondyly with short pedicles, vertebral scalloping, and interpediculate narrowing. There may be associated spinal foraminal and canal compromise.

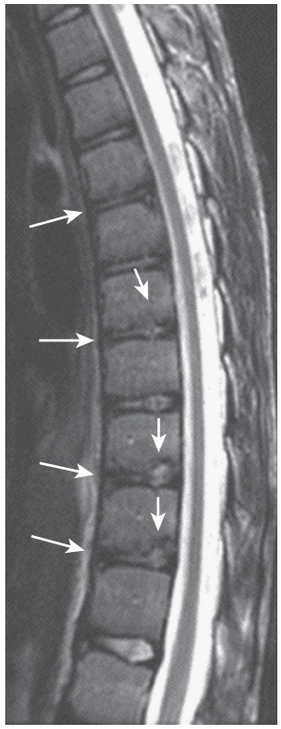

Figure 9-18. Scheuermann disease with multilevel, irregular thoracic disk space narrowing (*long arrows*) and Schmorl's nodes (*short arrows*).

Mucopolysaccharidosis

Mucopolysaccharidosis may be associated with craniocervical abnormalities (e.g., Morquio syndrome; Fig. 9-21). They include odontoid hypoplasia, occipital hypoplasia, ligamentous laxity, AA instability, and dural sac stenosis (mucopolysaccharide deposition with fibrosis; Fig. 9-22). Foraminal and spinal canal encroachment may occur. Other vertebral anomalies are platyspondyly, beaking, wedging, gibbus deformity, and kyphoscoliosis.

Down Syndrome

Down syndrome may be complicated by craniocervical instability, such as odontoid hypoplasia, os odontoideum, atlanto-occipital (AO) subluxation, or AA subluxation (see "Craniocervical Anomalies"; Figs. 9-23 and 9-24). Scoliosis, degenerative cervical spine disease, tall vertebral bodies, vertebral fusions, and subluxations at other levels may also occur.

Spondyloepiphyseal Dysplasia

Spondyloepiphyseal dysplasia (SED) occurs as a congenita or tarda form. In the congenita form there is dwarfism, thoracolumbar kyphosis, lumbar lordosis, platyspondyly, and odontoid hypoplasia with AA instability. The tarda form of SED consists of platyspondyly, dwarfism, and early degenerative spine and hip disease. Other skeletal dysplasias associated with spinal abnormalities include diastrophic dysplasia, metatropic dysplasia, spondylometaphyseal dysplasia, Kneist dysplasia, Larsen syndrome, chondrodysplasia punctata, craniometaphyseal dysplasia, osteogenesis imperfecta, osteopetrosis, and Marfan syndrome.

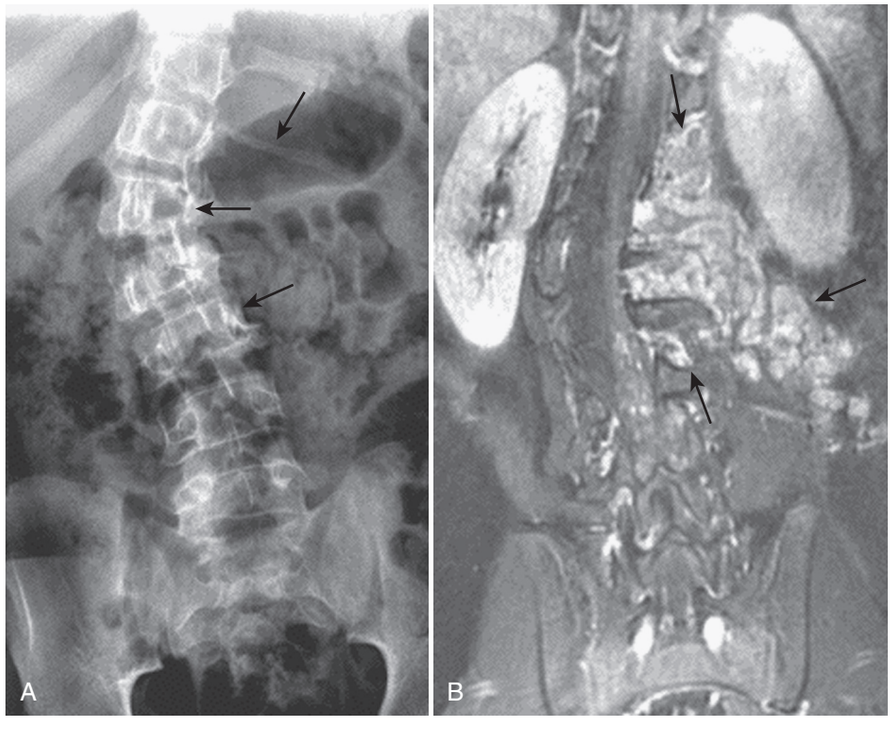

Figure 9-19. A, Neurofibromatosis-1 with short-segment right lumbar scoliosis plus vertebral and rib deformities (*arrows*) on frontal plain film/computerized radiograph. **B,** Enhancing paraspinal plexiform neurofibroma (*arrows*) with foraminal extension is shown on coronal gadolinium-enhanced T1-weighted MR image along with other small intradural enhancing nerve sheath tumors.

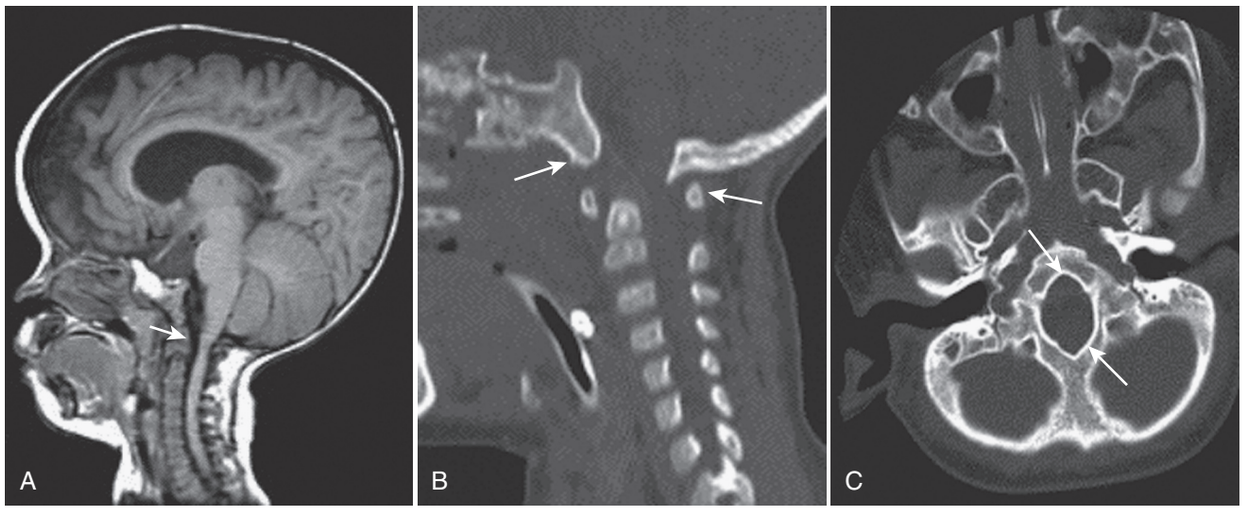

FIGURE 9-20. Achondroplasia, basilar invagination, and foramen magnum plus cervical spinal stenosis (*arrows*) on sagittal T1-weighted MR image (**A**), sagittal reformatted CT scan (**B**), and an axial CT scan (**C**). Also, there is characteristic macrocephaly and ventriculomegaly.

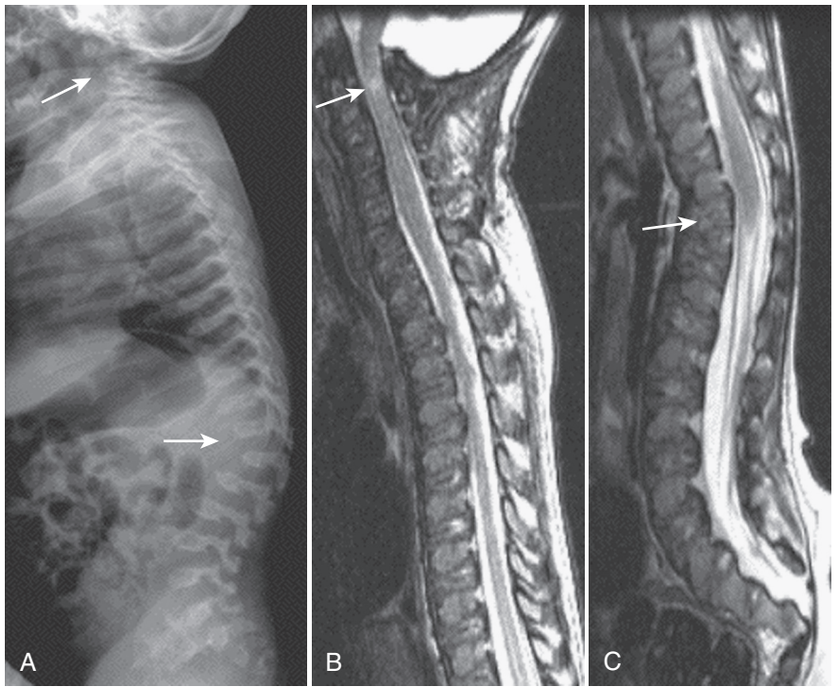

FIGURE 9-21. A, Morquio syndrome with craniocervical instability (*upper arrow*) plus thoracolumbar kyphoscoliosis (*lower arrow*) on a lateral plain film/computerized radiograph. **B** and **C,** Sagittal T2-weighted MR images show upper cervical dural sac stenosis with hyperintense cord injury (*arrow* in **B**) along with ventral cord deformity at the level of the kyphosis (*arrow* in **C**).

Craniocervical Anomalies

The craniocervical junction (CCJ) consists of the basiocciput, the atlas (C1) and axis (C2), and the ligaments of the AO and AA articulations. Imaging evaluation of this region often requires PF/CR, flexion-extension PF/CR or fluoroscopy, CT, and MRI.

A number of landmarks may be helpful in evaluating the CCJ. McRae's line defines the plane of the foramen magnum, and the dens tip should always be below it. The predental space in infants and young children (anterior atlas–dens gap) varies from 3 to a maximum of 5 mm in flexion with a 2-mm excursion from extension to flexion. The gap is normally less than 3 mm in adolescents and adults. The postdental space (dens–posterior atlas gap or dens–posterior foramen magnum gap) is at least 15 mm in children and 19 mm in adults. At the level of C1, the spinal canal area, according to the Steel rule of thirds, should be composed of one third dens, one third cord, and one third safe zone. The dens tip should align with tip of the clivus (basion) and these two structures should not be separated by more than 1 cm.

Common anomalies of the CCJ include basilar invagination, the Klippel-Feil anomaly, occipitalization of the atlas, odontoid anomalies, and craniocervical instability. CCJ anomalies may manifest clinically as torticollis, craniofacial or craniocervical dysmorphism, limitation of motion, headache or neck pain, neck mass, or clicking. Kyphosis and scoliosis may also be seen. Patients may also be presented with symptoms or signs related to hindbrain, cervical cord, or vertebrobasilar compromise. Such abnormalities may be discovered after recent or remote trauma.

Basilar Invagination

Basilar invagination refers to an occipital dysplasia with upward displacement of the margins of the foramen magnum anteriorly, posteriorly, laterally, or combined (Fig. 9-25 and 9-26). The odontoid is superiorly displaced relative to McRae's line. In addition the posterior fossa may be of small volume with an irregularly shaped foramen magnum and a short clivus. Basilar invagination may be (1) primary (i.e., developmental) and associated with other craniocervical anomalies or syndromes or (2) secondary (i.e., basilar impression) and associated with osteochondral dysplasias or metabolic disorders (e.g., rickets, fibrous dysplasia, achondroplasia, the mucopolysaccharidoses, osteogenesis imperfecta, osteomalacia, cleidocranial dysplasia). Basilar invagination may produce neural, CSF, or vascular compromise. There may be an associated Chiari I malformation, hydrocephalus, or hydrosyringomyelia.

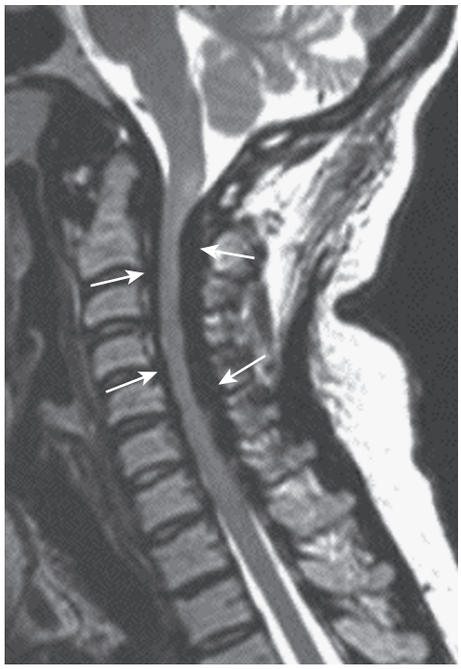

Figure 9-22. Scheie-type mucopolysaccharidosis with cervical dural/epidural hypointense thickening (*arrows*), dural sac stenosis, and cord thinning.

Klippel-Feil Anomaly and Syndrome

The Klippel-Feil *anomaly*, which results from failure of segmentation, manifests as bony fusion of the cervical spine at one or more levels (see Figs. 9-4 and 9-26). The triad of low posterior hairline, short webbed neck, and limitation of neck motion represents the Klippel-Feil *syndrome*. Sprengel's deformity of the scapula and a bridging omovertebral bone may also be present in Klippel-Feil syndrome. Other associated anomalies are genitourinary, cardiac, and musculoskeletal (e.g., limbs and digits). The spinal involvement may include posterior element abnormalities, occipitalization of the atlas, basilar impression, dens anomalies, and scoliosis. Chiari I malformation, hydrosyringomyelia, neurenteric cyst, or diastematomyelia may occur. Hypermobility and instability at unfused segments and early degenerative disease may lead to foraminal or spinal canal stenosis, osteophytic spurs, subluxation, facet arthropathy, or disk herniation.

Occipitalization of the Atlas

Occipitalization of the atlas refers to complete or partial fusion of the atlas to the occiput, which may be bony or fibrous (see Fig. 9-26). Usually, the anterior arch is assimilated into the anterior rim of the foramen magnum. The involvement may also include the posterior arch or lateral masses. Associated anomalies are odontoid hypoplasia, basilar invagination, AA instability, and Klippel-Feil anomaly.

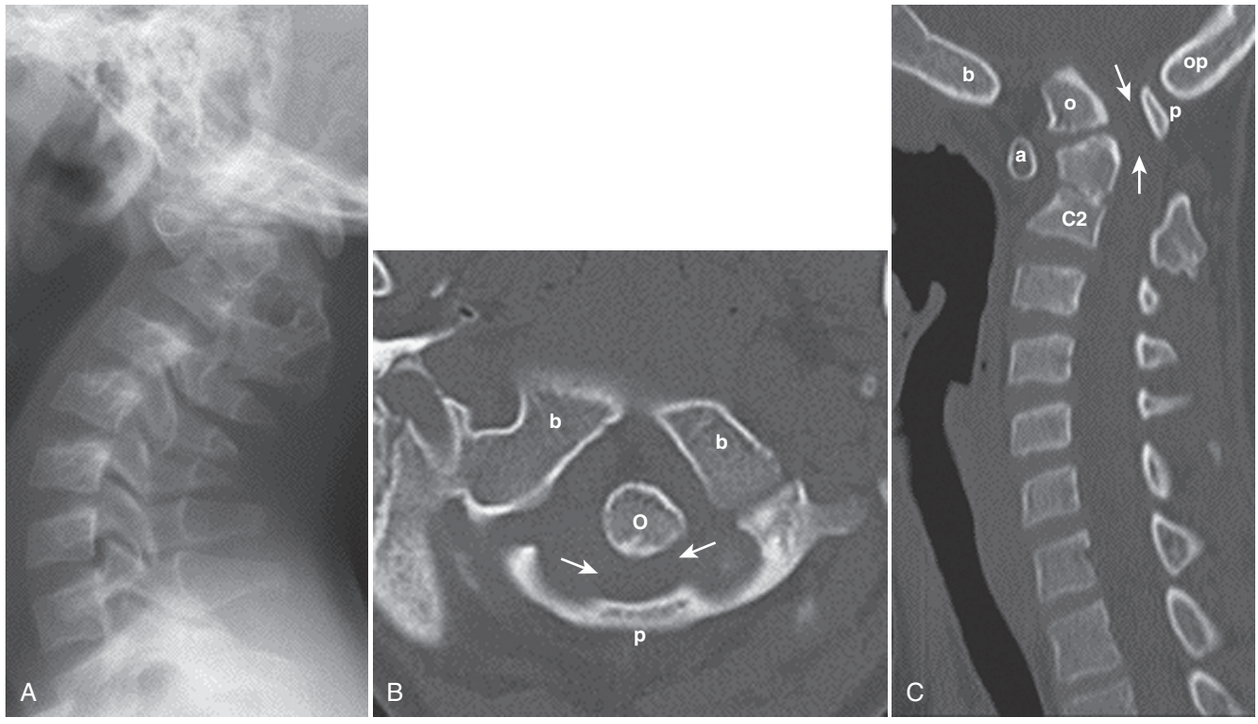

Figure 9-23. Lateral plain film/computerized radiograph (**A**), axial CT scan (**B**), and sagittal reformatted CT scan (**C**) showing Down syndrome with hypoplastic dens, os odontoideum (o), atlantoaxial instability, and post-dental canal stenosis (*short arrows*) with probable cord compression; C2, axis; a, anterior arch of atlas; p, posterior arch of atlas; b, basion; op, opisthion.

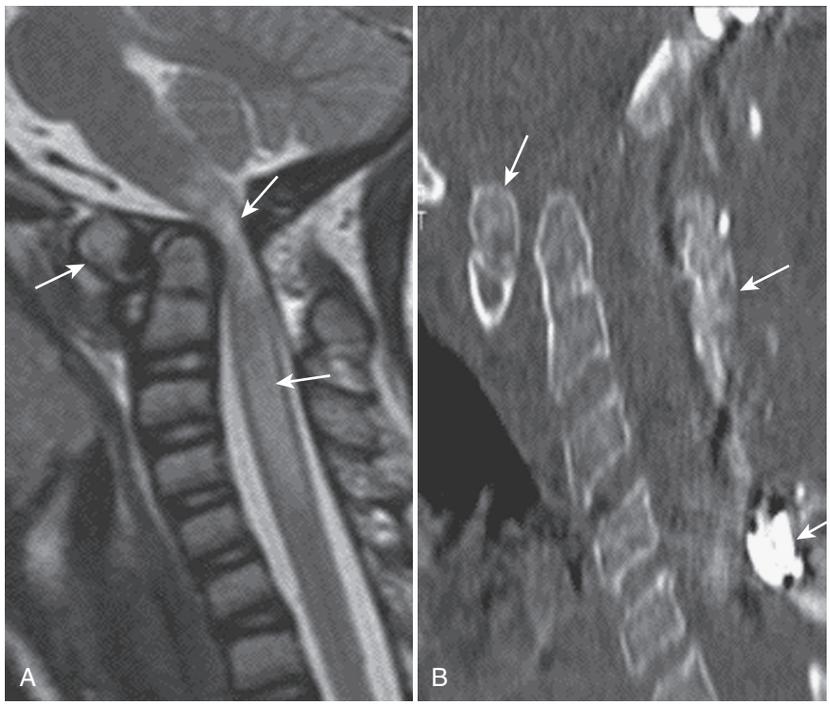

FIGURE 9-24. **A,** Sagittal T2-weighted MR image showing Down syndrome with hypoplastic dens, os odontoideum (*anterior arrow*), and atlantoaxial dislocation with high-intensity cervical spinal cord compressive injury (*posterior arrows*). **B,** Sagittal postoperative reformatted CT scan shows the stabilized anomaly, including the os odontoideum (*upper arrow*), decompressed canal, and metallic instrumentation plus bony fusion (*posterior arrows*).

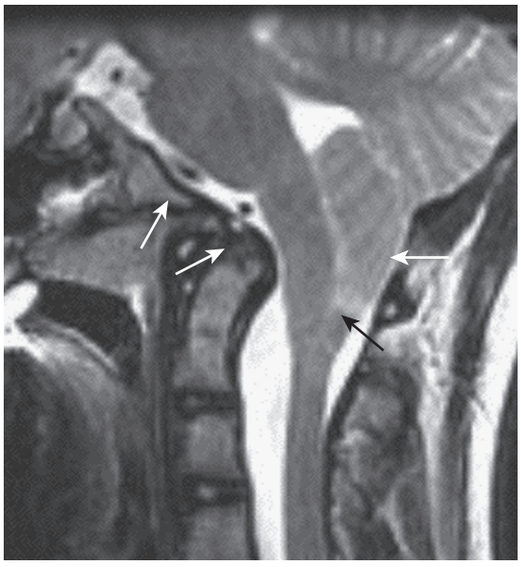

FIGURE 9-25. Basilar invagination and Chiari I malformation on sagittal T2-weighted MR image with short clivus and high dens (*anterior arrows*) plus low tonsils and low cervicomedullary junction (*posterior arrows*).

Odontoid Anomalies

Anomalies of the odontoid include aplasia, hypoplasia, and the os odontoideum (see Figs. 9-23 and 9-24). Aplasia is rare and causes severe AA dislocation. Hypoplasia leads to a short dens. Os odontoideum is a proatlas remnant or represents hypertrophy of the ossiculum terminale. Usually, there is odontoid hypoplasia, and the ossicle is located near the dens tip or the basion and lacks a normal dens fusion line. Hypertrophy of the anterior arch and hypoplasia or clefting of the posterior arch are often present. AA or occipitoaxial instability commonly occurs. Odontoid anomalies may be idiopathic or may be associated with skeletal dysplasias such as Morquio syndrome, Down syndrome, SED, and Klippel-Feil anomaly.

Craniocervical Instability

Craniocervical instability includes translational or rotary AA instability and AO instability. Craniocervical instability often results from ligamentous deficiency or insufficiency (e.g., transverse ligament in AA instabilities) and is commonly associated with odontoid anomalies (as discussed earlier). AA and AO instabilities most commonly occur with Down syndrome (see Figs. 9-23 and 9-24). Other common causes are the skeletal dysplasias (e.g., Morquio syndrome, SED), rheumatoid arthritis, and trauma. Rotary AA instability includes displacement, subluxation, or dislocation and produces torticollis. It may be spontaneous or related to trauma, infection, or CCJ anomalies (e.g., odontoid anomalies, Klippel-Feil anomaly).

Spinal Vascular Anomalies

Vascular anomalies of childhood may involve the paraspinal soft tissues, bony spinal column, spinal neuraxis, meninges, or multiple structures. The Mulliken and Glowacki biologic classification categorizes cutaneous and muscular vascular anomalies as vascular malformations (e.g., lymphatic, venous, arteriovenous), vascular tumors (i.e., hemangiomas), or angiodysplastic syndromes. These are covered in greater detail in Chapter 10. Vascular anomalies of the CNS have traditionally been classified as arteriovenous malformations (AVMs), developmental venous anomalies, cavernous malformations, telangiectasias, and aneurysms; these are covered in Chapter 8.

Intradural spinal vascular anomalies are usually AVMs or arteriovenous fistulae (AVFs) and are classified according to the anatomic site of origin or involvement. They may be classified as spinal cord AVMs (intramedullary), spinal dural AVFs, or metameric AVMs (Cobb syndrome), the last involving any or all layers of a spinal segment from the spinal cord to the skin. In spinal

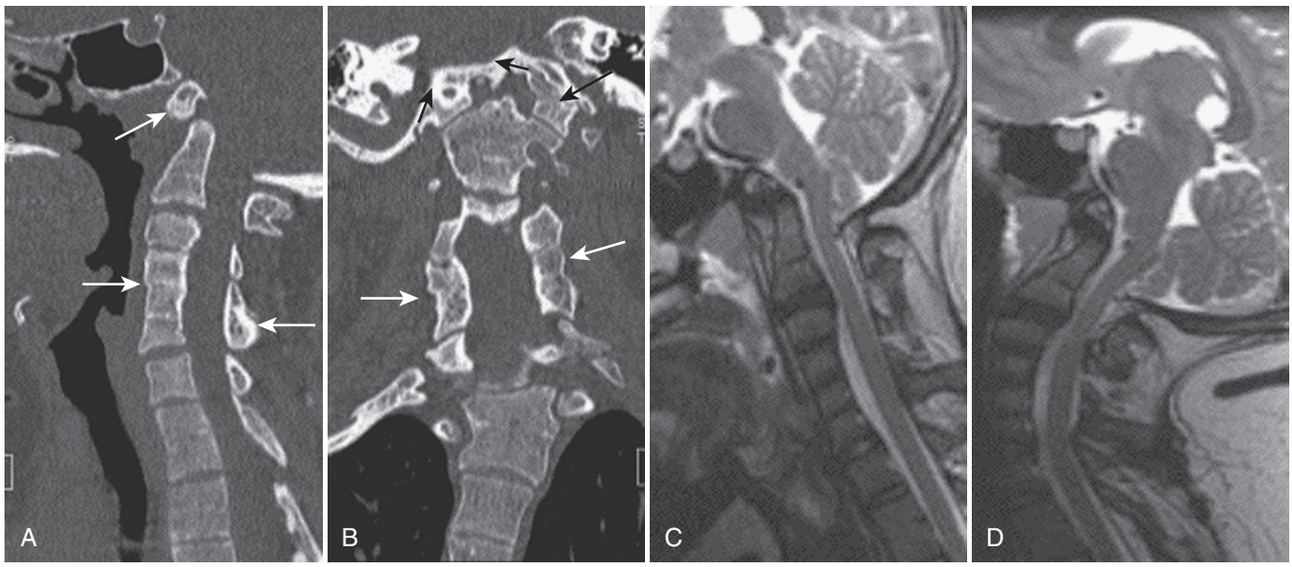

FIGURE 9-26. Sagittal (**A**) and coronal (**B**) reformatted CT scans showing Klippel-Feil anomaly, occipitalization of the atlas, and cervical spinal stenosis, including fused cervical segments (*lower arrows*), fusion of atlas to the occiput (*upper black arrows*), and a small foramen magnum and C1 canal. Flexion (**C**) and extension (**D**) T2-weighted sagittal MR images show no translational craniocervical instability.

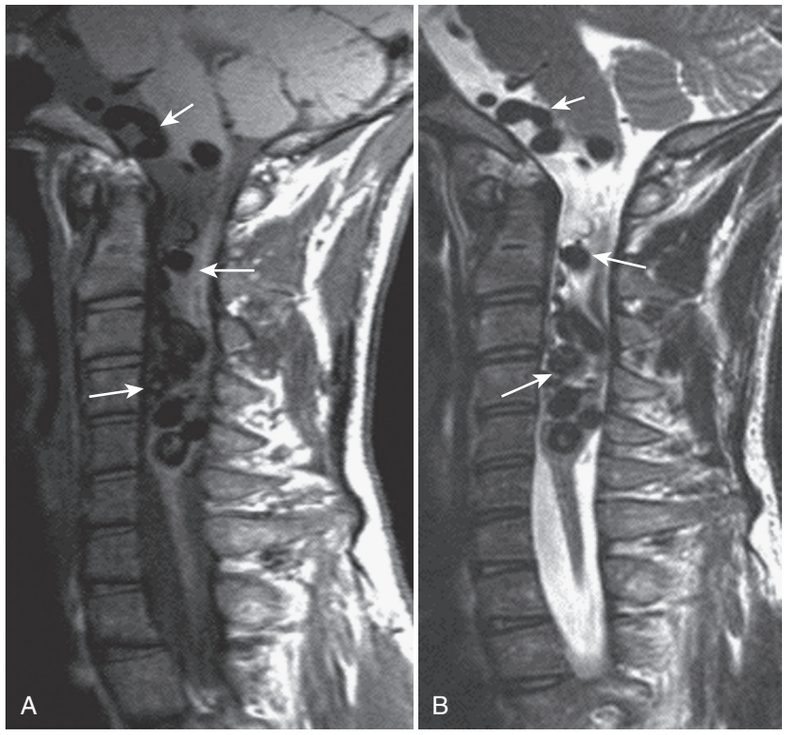

FIGURE 9-27. Cervical spinal cord arteriovenous malformation with high-flow vascular low intensities (*arrows*) on sagittal T1-weighted (**A**) and T2-weighted (**B**) MR images.

AVMs that are "high-flow" malformations, MRI may show nodular, serpiginous signal voids without tumor parenchyma, hemorrhage (subarachnoid or intramedullary), cord edema, infarct, myelomalacia, syrinx, or atrophy (Fig. 9-27). Spinal AVFs may be "high-flow" or "low-flow" malformations. Spinal angiography is necessary for full evaluation of the vascular anomaly in anticipation of surgery or interventional therapy. Cavernous angiomas of the spinal cord are rare and may manifest as hemorrhage (subarachnoid or intramedullary) or myelopathy.

ACQUIRED ABNORMALITIES

Trauma

Spinal Fractures

Spinal fractures occur less commonly in childhood than in adulthood and may be related to vehicular accidents, falls, diving, sports, recreation, or child abuse. In infants and young children the injuries are usually upper cervical. Owing to the relative larger head size, spinal immaturity, and higher fulcrum for

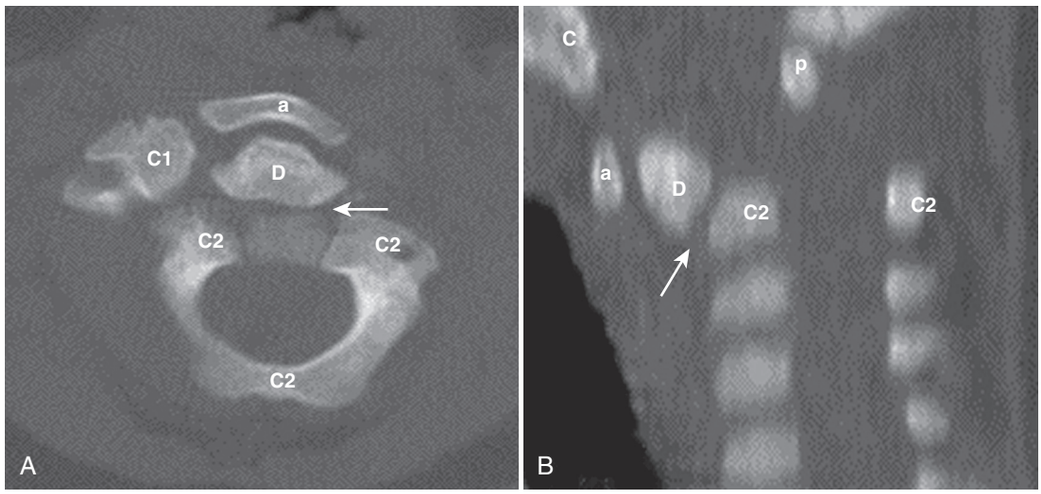

FIGURE 9-28. Infant dens fracture type 2 (*arrows*) with anterior atlantoaxial displacement/dislocation on axial (**A**) and sagittal (**B**) reformatted CT scans; a, anterior arch of C1; C, clivus; C1, atlas; C2, axis; D, dens; p, posterior arch of C1.

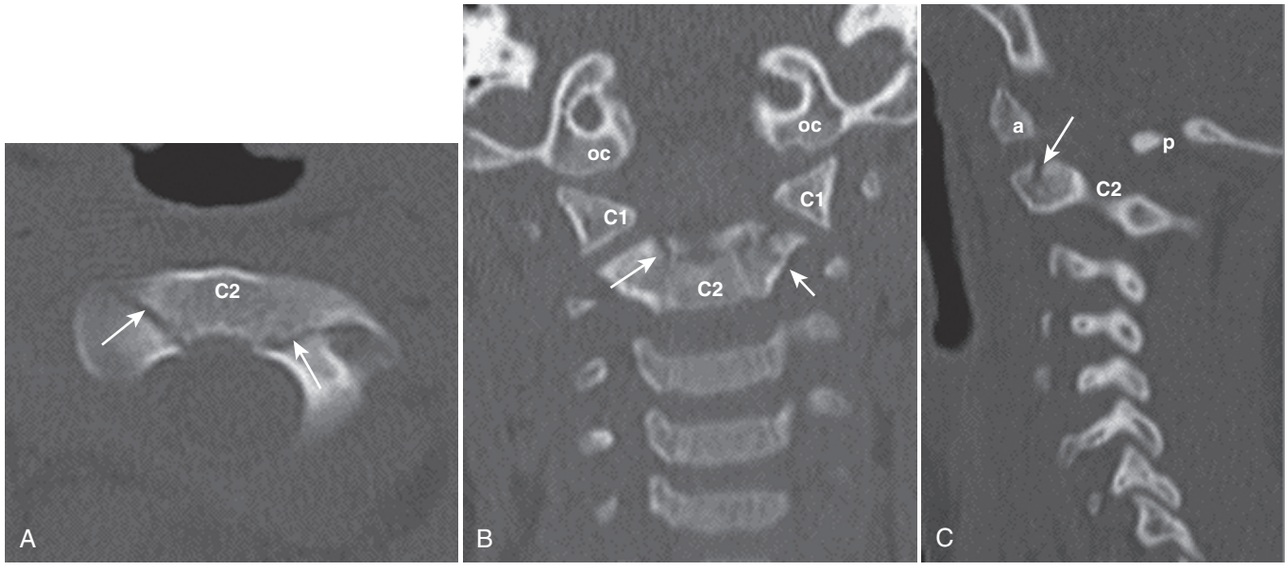

FIGURE 9-29. Hangman's C2 fracture (*arrows*) on axial (**A**), coronal (**B**), and parasagittal (**C**) reformatted CT scans; a, anterior arch of C1; C1, atlas; C2, axis; oc, occipital condyles; p, posterior arch of C1.

flexion-extension (above C2-C3), injuries in infants and young children are usually upper cervical. The spectrum includes fractures of the synchondroses of the atlas, axis, or dens and AA or occipitoatlantal (OA) dislocations (Figs. 9-28 to 9-30). After closure of the synchondroses by 8 to 10 years of age, the fulcrum shifts caudally and injuries tend to occur at the mid- to lower cervical levels (adult pattern). In the patient with spine injury, PF/CR may be performed initially with the patient properly immobilized. However, CT (e.g., MDCT) with sagittal and coronal reformatting has become the standard. MRI (with STIR) is used for further evaluation to assess for intraspinal hematoma, spinal cord injury, or ligamentous damage (Fig. 9-31).

Spinal Injury

Spinal injury results from one or a combination of basic mechanisms. *Hyperflexion* may lead to posterior ligamentous sprain, bilateral or unilateral interfacet dislocation, compression fracture, clay shoveler fracture, flexion teardrop fracture, dens fractures (see Fig. 9-28), or lateral mass fractures of C1 or C2 (i.e., lateral flexion). *Hyperextension* may lead to anterior ligamentous sprain, avulsion fracture of the anterior arch of the atlas, C1 posterior arch fracture, extension C2 teardrop fracture, laminar fracture, hangman's fracture (i.e., traumatic C2 spondylolisthesis; see Fig. 9-29), pillar fracture, odontoid fracture, or pedicle or lamina fracture. *Axial compression* may produce Jefferson C1 fracture or burst fracture of the vertebral bodies. *Distraction forces* may result in AA or AO disassociation or chance fractures. *Translational or rotary injury* may produce AA or AO subluxation/dislocation, unilateral or bilateral facet subluxation, or fracture/dislocation (see Fig. 9-30).

Spinal injury in *neonates and young infants* may occur with birth (e.g., breech delivery), accidents, falls, or child abuse. These injuries occur primarily in the cervical spine and may result in fractures of the neurocentral synchondroses or dens

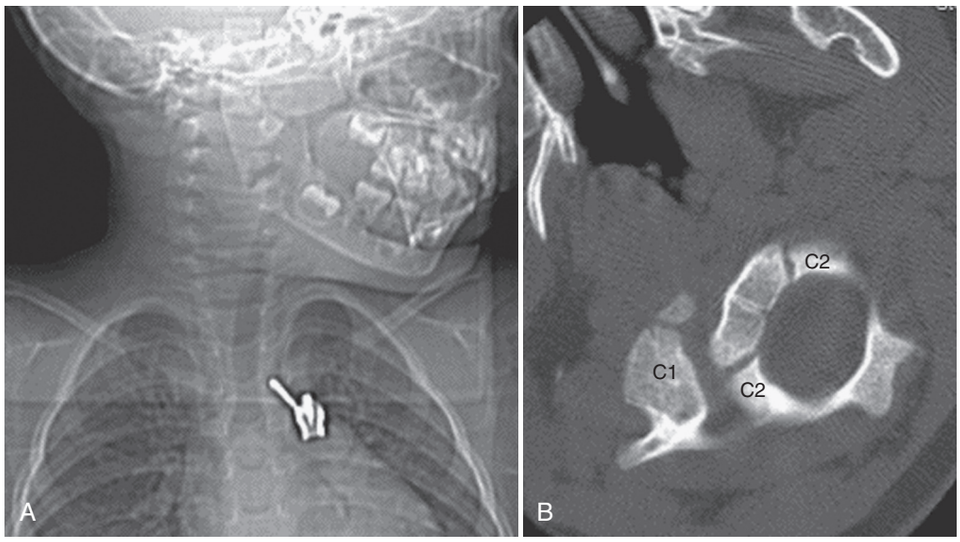

FIGURE 9-30. Painful torticollis on frontal plain film/computerized radiograph (**A**). Rotary C1 to C2 fixation/subluxation on axial CT scan (**B**), which also shows clockwise offset of C1 lateral mass relative to C2 lateral mass.

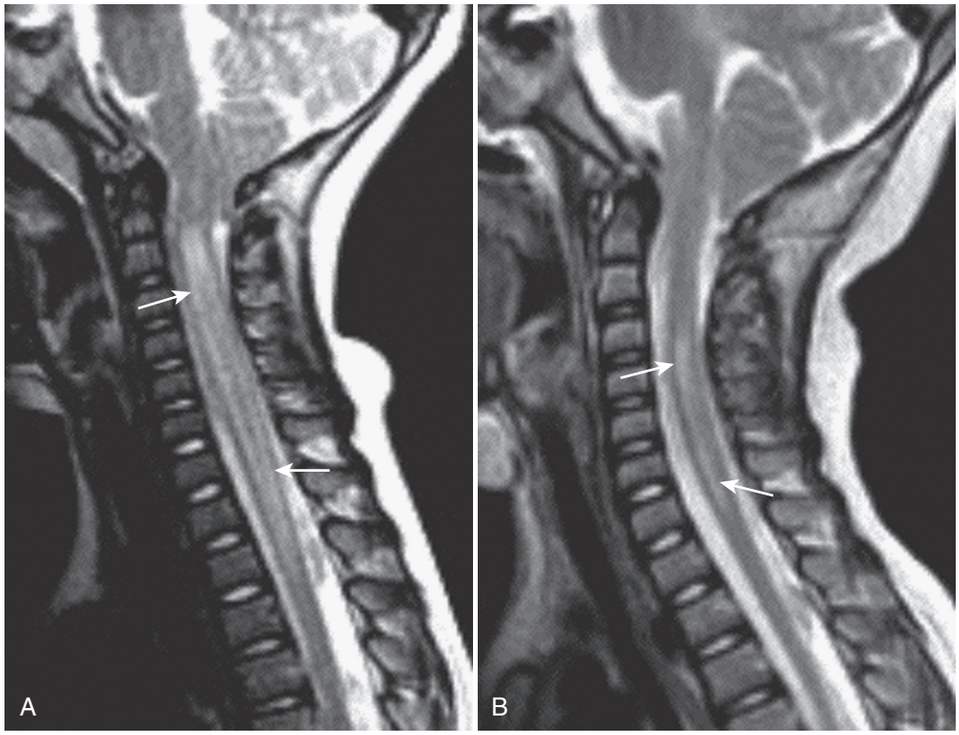

FIGURE 9-31. Sagittal T2-weighted MR images showing Chiari I malformation with trauma and acute hyperintense cervical cord edema (*arrows* in **A**) followed by chronic hyperintense syrinx formation (*arrows* in **B**). The differential diagnosis includes myelitis, demyelination, and ischemia, with tumor less likely.

as well as dislocations of the AO or AA articulations (see Figs. 9-28 and 9-29). Occasionally there may be an associated epidural, subdural, or subarachnoid hemorrhage. Spinal cord injury without radiographic abnormality (SCIWORA), which may occur with reversible spinal column dislocation, includes contusion, edema, avulsion, or transaction (see Fig. 9-31). Because of injury to the cervicomedullary junction, there may be respiratory arrest with otherwise unexplained hypoxic-ischemic brain injury (Fig. 9-32). PF/CR and CT findings are often negative, and MRI is needed for the diagnosis. Brachial plexus injury (e.g., shoulder dystocia) may lead to Erb palsy or Klumpke paralysis. As a result, dural tear with CSF leakage may be associated with nerve root laceration and pseudomeningocele formation.

In *older infants and children up to age 8 years*, injuries to the cervical spine also often result in fractures of the apophyses and synchondroses, including avulsions and separations of the dens, axis body, and atlas ring. The Jefferson fracture represents axial compression fractures of the anterior and posterior C1 arches, often with outward displacement of the articular masses. Less common C1 fractures include posterior arch fractures and anterior arch avulsions. Odontoid fractures occur often at the subdental synchondrosis (type 2) and less commonly at the tip (type 1) or axis body (type 3). Hangman's fracture is a bilateral hyperextension

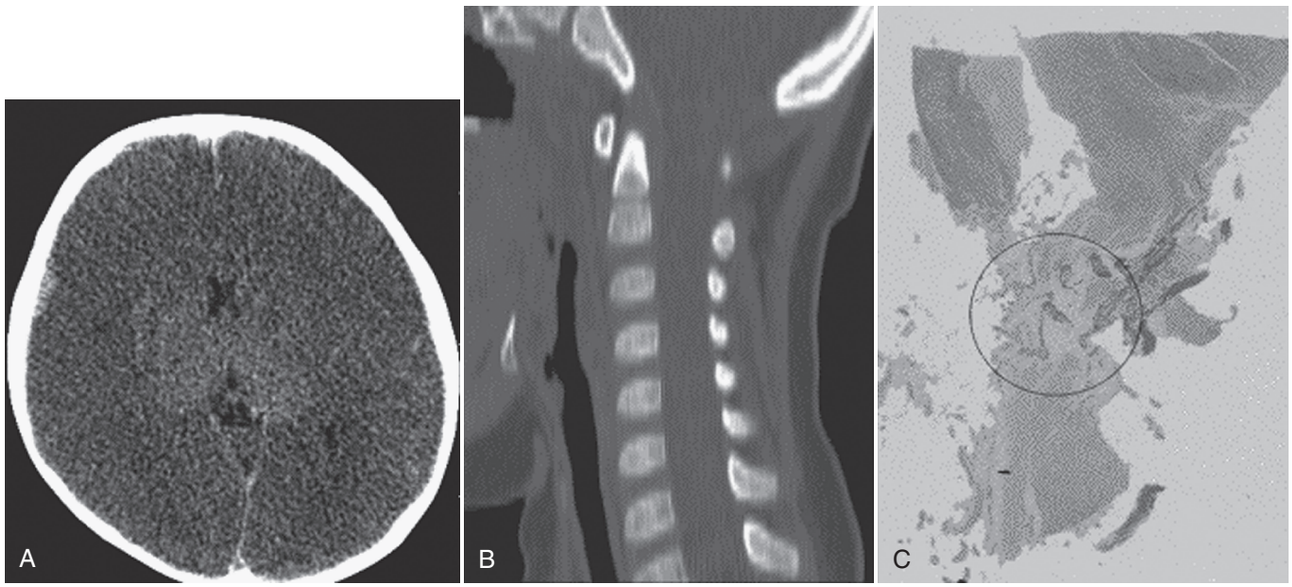

FIGURE 9-32. Spinal cord injury without radiographic abnormality (SCIWORA). **A,** axial CT scan shows hypoxic-ischemic brain injury and subdural hemorrhage. **B,** Findings on cervical spine CT scan are negative. **C,** Postmortem microsection shows partial cervicomedullary transection (*circle*).

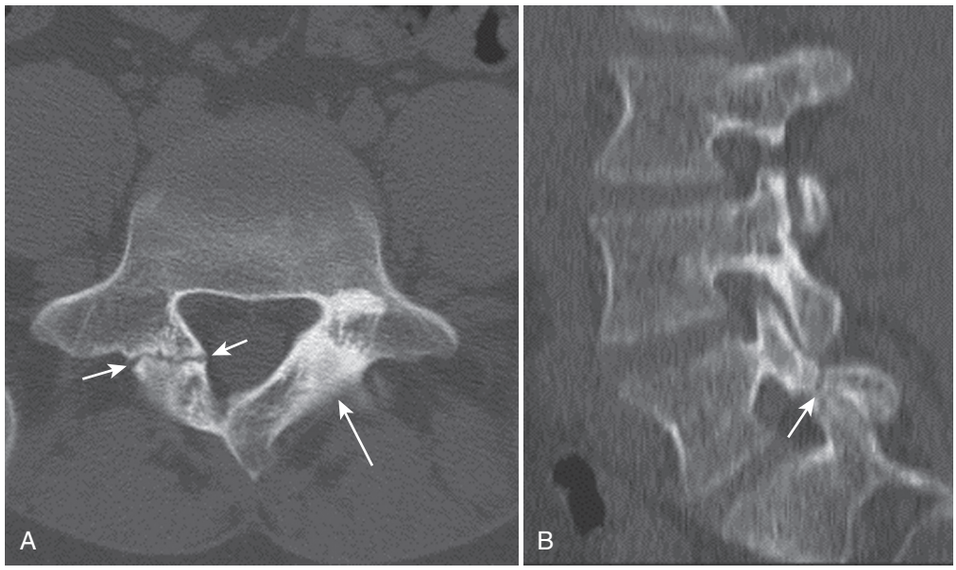

FIGURE 9-33. Spondylolysis on axial (**A**) and reformatted parasagittal (**B**) CT scans, with a hypodense pars defect on the right (*short arrows*) and more hyperdense sclerosis on the left (*long arrow*).

fracture of the C2 pars interarticularis. AA or AO instability may be associated with these fractures. AA and AO dislocations may also occur without obvious fracture and may be associated with severe spinal cord injury. In the *juvenile and adolescent*, cervical spine injuries tend to follow the adult patterns. Thoracolumbar spinal injury also occurs in childhood. The spectrum includes compression or chance fractures (horizontal body and neural arch fracture) associated with hyperflexion seat belt trauma, and axial burst fractures from falls.

Spinal Cord Injury

Spinal cord injury, including cord compression from spinal malalignment, bony fragments, disk herniation, and intraspinal hematoma, is best assessed with MRI. STIR imaging is particularly helpful in demonstrating ligamentous injury. Cord injury includes contusion, hemorrhage, edema, avulsion, and transection (see Fig. 9-31). MRI also assesses chronic sequelae, such as posttraumatic cyst or syringomyelia, myelomalacia, arachnoiditis, arachnoid cyst, and neuroarthropathy (see Fig. 9-31).

Spondylolysis and Spondylolisthesis

Pars interarticularis defects (i.e., spondylolysis) are a common cause of back pain in childhood. Anterior slippage of the upper vertebral body upon the lower one (i.e., spondylolisthesis) is a common complication. Bilateral in most cases, spondylolysis usually occurs at L5 or L4. Although it is often associated with repetitive trauma, a developmental predisposition is likely. A dysplastic type is characterized by hypoplasia/aplasia of the L5 neural arch and S1 apophyseal joints. The extent of slippage may be assigned as Meyerding grade 1 (up to 33%), grade 2 (up to 66%), grade 3 (up to 99%), or grade 4 (100% with spondyloptosis). Although these problems are often detected by plain films or RI (e.g., SPECT), CT is preferred for complete evaluation (Fig. 9-33). MRI helps evaluate for other, or additional, causes of back pain (e.g., disk herniation, synovial cyst).

Disk Herniations and Calcifications

Herniations usually occur in adolescence from trauma (e.g., athletic activity) and are best shown by MRI. These usually arise at L4-L5 or L5-S1 and may be associated with a slipped vertebral apophysis. CT best shows the latter. Disk calcification in childhood is rare and usually of unknown etiology. It occurs mostly in boys at the cervical or thoracic level. Symptoms include pain, stiffness, and decreased motion. Anterior or posterior herniation may also occur. Although possibly detected by plain film, it is best evaluated with CT and MRI.

Infection and Inflammation

Infection may involve the disk, vertebral body, paravertebral soft tissues, epidural space, meninges, or spinal neuraxis. Infectious processes occurring during childhood include spondylitis (diskitis, vertebral osteomyelitis), sacroiliac pyarthrosis, epidural abscess or empyema, meningitis, arachnoiditis, myelitis, and spinal cord abscess. These are all best evaluated with MRI.

Infectious Spondylitis

Infectious spondylitis in childhood is most often of hematogenous origin but may also arise from contiguous spread or direct inoculation. The infecting agent is usually bacterial (e.g., *Staphylococcus aureus*) or viral. The immature and highly vascularized disk is often initially involved (i.e., diskitis). Extension with vertebral end plate involvement (i.e., osteomyelitis) is common. The lumbar level is the most common site. PF/CR findings are often negative in early infection, but results of bone scan (e.g., SPECT) may be positive. CT is more sensitive than PF/CR, but MRI is the choice for complete evaluation and as a guide for subsequent abscess aspiration or biopsy by CT. Disk space narrowing, end plate irregularities or erosions, and sclerosis may be present on CT. Additional MRI findings are T1 hypointensity, T2 hyperintensity, and gadolinium enhancement within the disk, vertebral body, and paraspinal soft tissues (Fig. 9-34). There may be an associated epidural or paraspinal abscess, or, rarely, meningitis. Sequelae include disk degeneration, vertebral destruction, osseous bridging, scoliosis, kyphosis, and Schmorl nodes.

Granulomatous spondylitis usually results from *Mycobacterium* tuberculosis, with a predilection for children from underserved or developing areas. Thoracolumbar involvement is common and may be primary or secondary (spread from other organs). Insidious onset and gradual progression are characteristic. Imaging shows anterior vertebral erosion or extensive vertebral destruction, with or without disk loss, paraspinal masses (granuloma, abscess), and calcification (Fig. 9-35). Progression to kyphosis with gibbus deformity may also be present.

Sacroiliac Pyarthrosis

Pyogenic arthritis (e.g., due to *S. aureus* infection) of the sacroiliac joint may rarely occur during late childhood and may progress to ankylosis if treatment is delayed. It may be primary or an extension from contiguous osteomyelitis of the sacrum or ileum. The presentation is often nonspecific, consisting only of back, hip, or limb pain. PF/CR findings are often negative early, but bone scan results are usually positive. MRI provides definitive evaluation.

Epidural Abscess

Epidural abscess is uncommon in childhood. It may be hematogenous in origin or may arise as a direct extension from suppurative spondylitis (e.g., due to *S. aureus*). MRI demonstrates an extradural soft tissue mass that may extend over several segments. The collection is often T1-isointense to hypointense, and T2-hyperintense. Diffuse homogeneous enhancement corresponds with phlegmon. Rim enhancement represents a necrotic abscess. Associated findings of spondylitis (described earlier) may be present.

Meningitis

Bacterial, fungal, viral, or parasitic organisms may cause meningitis. The majority of cases are bacterial. MRI may demonstrate nonspecific, linear or nodular gadolinium enhancement of the meninges, spinal cord, or nerve roots (Fig. 9-36). Similar findings may be seen with neoplastic seeding (e.g., medulloblastoma).

Arachnoiditis

Arachnoiditis may occur after infection, subarachnoid hemorrhage, intraspinal injection (e.g., for anesthesia, chemotherapy), surgery, or trauma. MRI shows nerve root thickening and clumping, often with enhancement, and occasionally a mass (see Fig. 9-36). There may be associated hydrosyringomyelia or arachnoid cysts.

Myelitis

Myelitis, which refers to spinal cord inflammation, is often viral. Viruses associated with myelitis include herpesvirus, coxsackievirus, poliovirus, and human immunodeficiency virus. Myelitis may also be post-viral or post-vaccinial, as with acute disseminated encephalomyelitis (ADEM). Other rare causes of inflammatory myelopathy in childhood include autoimmune demyelination (e.g., multiple sclerosis) and vasculitis (e.g., systemic lupus erythematosus); it may also arise as a complication of systemic malignancy, chemotherapy, or radiotherapy. Devic syndrome is the association of myelitis with optic neuritis (see Chapter 8). MRI findings include intramedullary T2 hyperintensity, cord expansion, and enhancement. The differential diagnosis for such findings includes myelitis, demyelination (e.g., ADEM), trauma, ischemia, and tumor (see Fig. 9-31).

Spinal Cord Abscess

Although rare, spinal cord abscess may occur by direct spread (e.g., dermal sinus; see Fig. 9-10), remotely by hematogenous or lymphatic spread, or in the immune-compromised child.

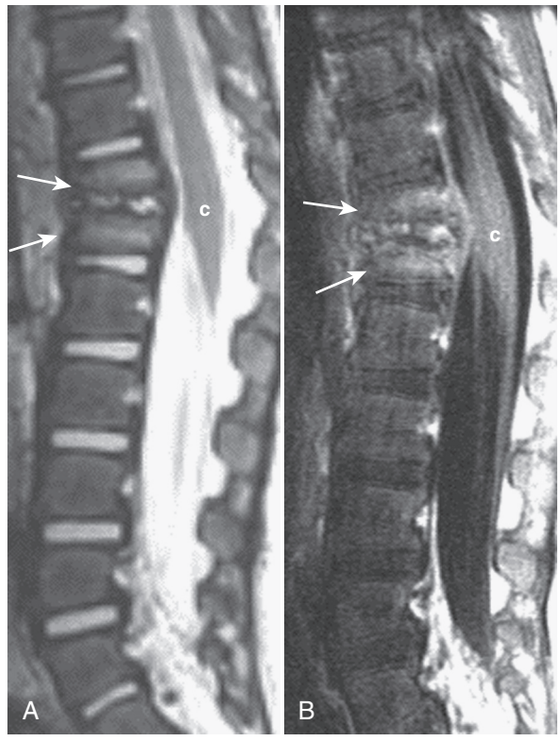

FIGURE 9-34. Sagittal T2-weighted (**A**) and gadolinium-enhanced T1-weighted (**B**) MR images show suppurative thoracolumbar diskitis/osteomyelitis (*arrows*) with disk space and end plate involvement plus T2-weighted hyperintensity and enhancement; c, conus medullaris.

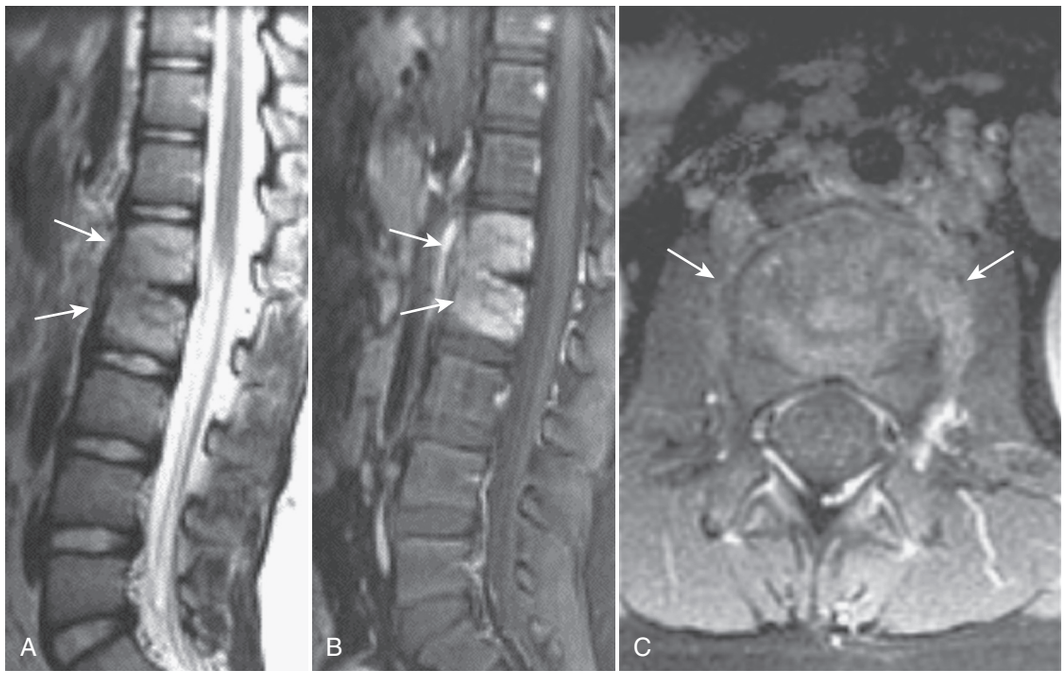

FIGURE 9-35. Lumbar tuberculous spondylitis. Sagittal T2-weighted (**A**) and gadolinium-enhanced sagittal (**B**) and axial (**C**) T1-weighted MR images show disk space narrowing, end plate irregularity, and vertebral T2-weighted hyperintensity plus enhancement (*arrows*).

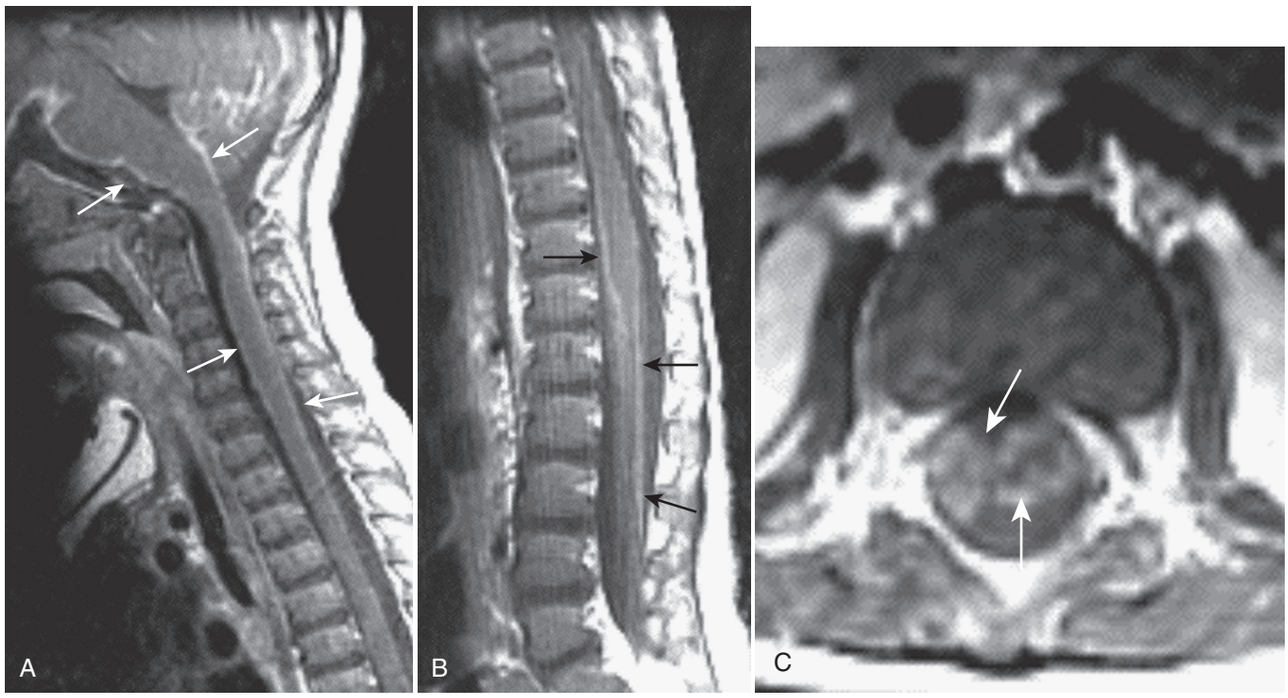

FIGURE 9-36. Tuberculous meningitis with intracranial and intraspinal involvement on sagittal (**A** and **B**) and axial (**C**) gadolinium-enhanced T1-weighted MR images, which show enhancement (*arrows*) along the brainstem, spinal cord, and nerve roots.

Neoplastic Conditions

Spinal tumors may be classified compartmentally (Table 9-1) as extradural (e.g., paraspinal, parameningeal), intradural (i.e., intrathecal, extramedullary), or intramedullary (i.e., spinal cord).

Extradural Tumors

Extradural, or parameningeal, tumors arise from the spinal column or paraspinal soft tissues. These tumors may spread to the spinal canal directly, by epidural venous extension, or by

Table 9-1. Neoplastic Spinal Lesions

Extradural tumors	Osteoid osteoma Osteoblastoma Osteochondroma Aneurysmal bone cyst Giant cell tumor Langerhans cell histiocytosis Leukemia and lymphoma Rhabdomyosarcoma Ewing sarcoma Fibromatosis Osteosarcoma Chondrosarcoma Chordoma Neuroblastoma Ganglioneuroblastoma Ganglioneuroma Primitive neuroectodermal tumor (PNET) Plexiform neurofibroma Metastases
Intradural (extramedullary) tumors	Schwannoma and neurofibroma Neoplastic seeding Developmental tumors Meningeal tumors (rare)
Intramedullary tumors	Astrocytoma Ganglioglioma Ependymoma Mixed glioma Glioblastoma PNET Hemangioblastoma Metastases

hematogenous, lymphatic, or CSF dissemination. This category includes benign and malignant bone and soft tissue tumors or tumor-like conditions of mesenchymal, neural crest, primitive neuroepithelial, and metastatic origins. In addition to CT and MRI, PET (e.g., PET-CT) and other nuclear imaging techniques are very helpful in the initial and follow-up evaluations of many of these tumors.

Benign Tumors of Mesenchymal Origin

Osteoid osteoma is a benign tumor with osteoid matrix and a fibrovascular nidus. A small percentage arise in the spine—most often lumbar, less often thoracic, and least often cervical—and manifest as pain, tenderness, and scoliosis. Neural arch involvement is typical. Plain films or CT may show a radiolucent nidus with calcification and surrounding sclerosis (Fig. 9-37). Increased radionuclide uptake is seen on bone scan. MRI may show extensive bone edema (T1-hypointense, T2-hyperintense), sclerosis or calcification (T1- and T2-hypointense), and the nidus (T1-isointense to hypointense, T2-hypointense or hyperintense, gadolinium-enhancing). The lesion may be treated by surgical excision or interventional ablation.

Osteoblastoma, also known as giant osteoid osteoma (> 2 cm), has a fibrovascular matrix with sclerotic osteoid mesenchyme and giant cells. It commonly occurs in the spine (e.g., cervical), is usually solitary, and typically involves the posterior elements. PF/CR or CT may show an expansile lytic lesion with bone matrix or calcific flecks. MRI shows T1 isointensity or hypointensity, T2 heterogeneity, and occasional hemorrhage. Treatment may be interventional therapy (e.g., embolization), surgical excision, or radiotherapy (e.g., for recurrence).

Osteochondroma is a benign osteocartilaginous exostosis that rarely occurs in the spine (e.g., cervical or thoracic posterior elements). It may be multiple (e.g., hereditary multiple osteochondromas). PF/CR or CT may show a bony projection with cartilaginous cap. MRI shows associated T1 isointensity or hyperintensity and T2 hyperintensity. Treatment is primarily surgical. Malignant degeneration (e.g., osteosarcoma or chondrosarcoma)

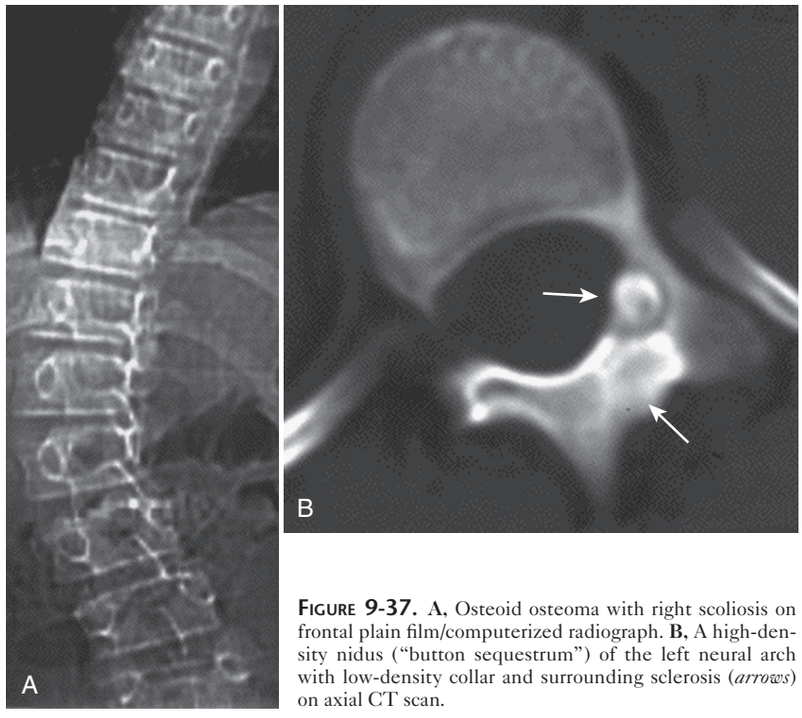

Figure 9-37. A, Osteoid osteoma with right scoliosis on frontal plain film/computerized radiograph. **B,** A high-density nidus ("button sequestrum") of the left neural arch with low-density collar and surrounding sclerosis (*arrows*) on axial CT scan.

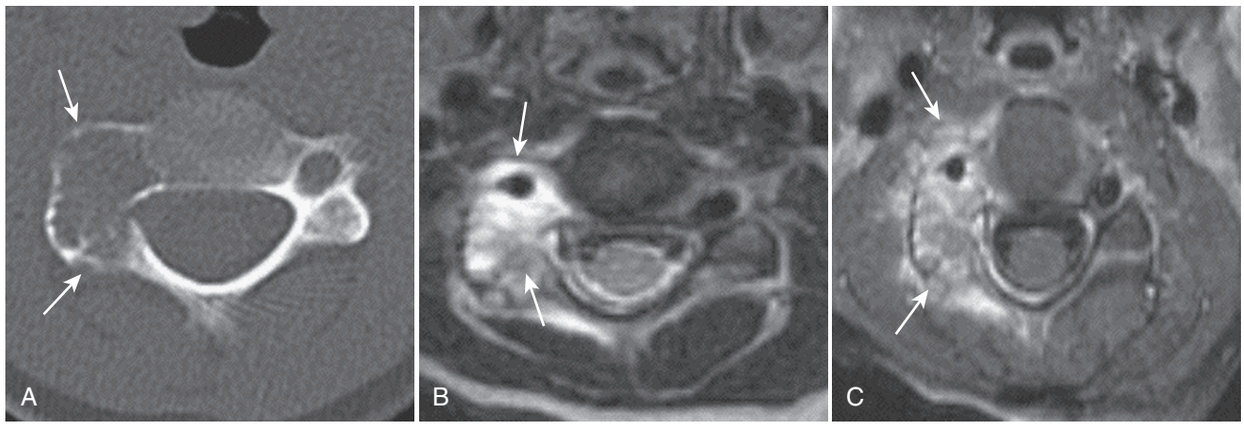

FIGURE 9-38. Aneurysmal bone cyst (*arrows*) of C3 neural arch on axial CT scan (**A**) and T2-weighted (**B**) and gadolinium-enhanced T1-weighted (**C**) MR images, which show lytic expansion, fluid levels, extensive enhancement, and vertebral artery involvement.

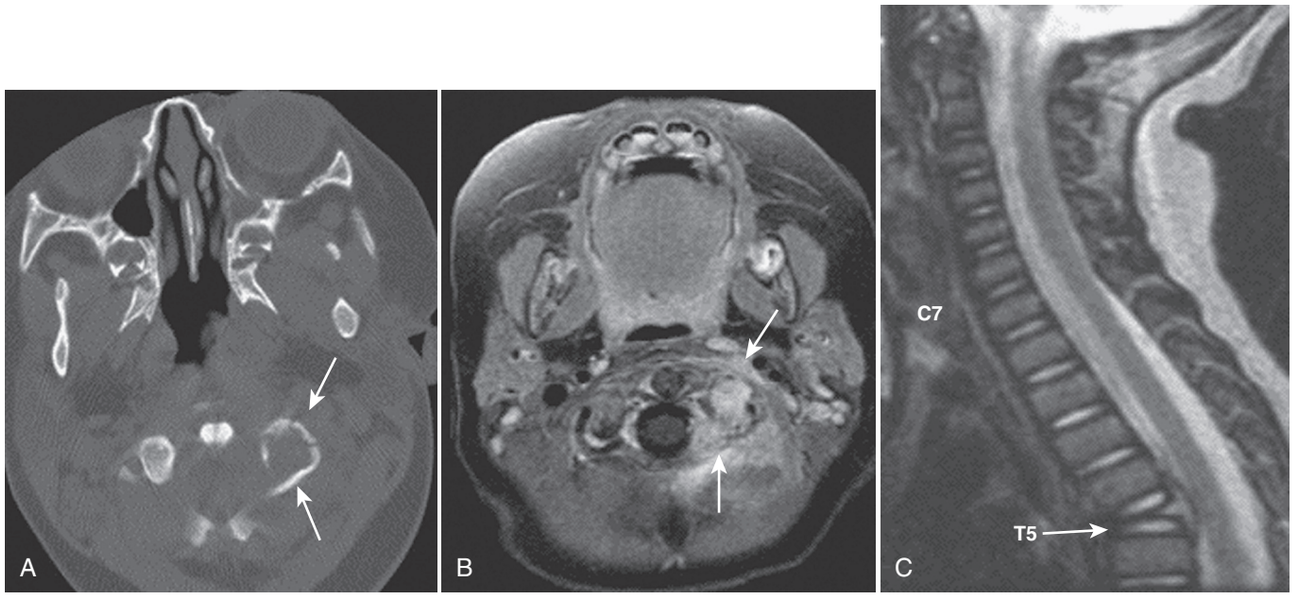

FIGURE 9-39. A, Axial CT scan shows a left C1 lateral mass lytic lesion in a patient with Langerhans cell histiocytosis with torticollis. **B,** Axial gadolinium-enhanced T1-weighted MR image shows lesion enhancement. **C,** Sagittal T2-weighted MR image shows T5 "vertebra planum" deformity (*arrow*).

is indicated by additional soft tissue mass, marrow involvement, a disorganized cap, or increased enhancement.

Aneurysmal bone cyst is a nonneoplastic bone lesion of non–endothelium-lined cavities filled with blood elements. It occasionally arises within the spine and tends to involve the posterior elements and adjacent vertebral body (Fig. 9-38). The cyst often expands into the paraspinal soft tissues or spinal canal. Aneurysmal bone cyst may occur with other lesions (e.g., giant cell tumor, osteoblastoma, chondroblastoma, nonossifying fibroma, fibrous dysplasia). PF/CR or CT may show an expansile lytic lesion with peripheral shell-like calcification and fluid-fluid levels. MRI additionally demonstrates variable intensities with varying stages of hemorrhage. Treatment is often a combination of intervention (i.e., embolization) and surgery (excision).

Giant cell tumor is an osteoclastoma composed of multinucleated giant cells, a fibroblastic stroma, and prominent vascularity. It rarely occurs in the spine (e.g., the sacrum). PF/CR or CT may show a lytic, expansile bone lesion breaking through the cortex. MRI additionally shows T1 isointensity or hypointensity, T2 isointensity or hyperintensity, associated hemorrhage or cysts, and gadolinium enhancement. Treatment is similar to that for other lesions mentioned here (e.g., osteoblastoma).

Malignant Tumors of Mesenchymal Origin

The subcategory malignant tumors or mesenchymal origin broadly includes the malignant "round cell tumors" of childhood that primarily or secondarily involve the reticuloendothelial system (e.g., Langerhans cell histiocytosis, leukemia, lymphoma, rhabdomyosarcoma, Ewing sarcoma, primitive neuroectodermal tumor [PNET], neuroblastoma). The round cell tumors have similar imaging patterns, including focal, multifocal, or diffuse involvement (e.g., marrow infiltration). Treatment for tumors in this category usually requires some combination of chemotherapy, radiotherapy, and surgery.

Langerhans cell histiocytosis describes a series of diseases characterized by abnormal histiocytes. One of the more classic forms of the disease is formerly known as "eosinophilic granuloma," which is seen in young children and often involves the lumbar and thoracic spine. PF/CR or CT may show circumscribed lytic lesions within the vertebral bodies or vertebral body collapse (i.e., vertebra plana), often without much of a soft tissue component (Fig. 9-39). Occasionally, a soft tissue mass extends into the spinal canal. MRI shows additional T1 isointensity or hypointensity, T2 hyperintensity, and gadolinium enhancement, especially with use of fat suppression (see Fig. 9-39).

Leukemia is the most common malignancy of childhood (e.g., acute lymphoblastic and acute monoblastic forms). There may be complications related to bone marrow infiltration, leukemic meningitis, or leukemic masses (chloromas). As with other round cell tumors, PF/CR may demonstrate diffuse bone marrow infiltration as osteopenia, permeative lytic destruction, or lucent bands. MRI of round cell tumors may additionally show hypercellular marrow infiltration as T1-hypointense and T2-isointense to hyperintense with gadolinium enhancement. In younger patients, it may be difficult to distinguish tumor infiltration of marrow from the hematopoietically active red marrow (also T1-hypointense, T2-isointense to hyperintense, and enhancing). Conversion to yellow marrow (increased fat content, therefore T1-hyperintense) occurs with increasing age as well as with the myelosuppressive effects of radiotherapy and chemotherapy. Marrow infiltration may then be more readily detected until there is red marrow rebound after therapeutic response (including after bone marrow transplantation). A mottled marrow pattern may represent combined tumor and treatment effects. Fat-suppression T2-weighted techniques (e.g., STIR) and fat suppression combined with gadolinium-enhanced T1-weighted sequences increase sensitivity and specificity for tumor (i.e., marked enhancement). CT may show chloromas as isodense to hyperdense, markedly enhancing masses that may be associated with bone destruction. MRI often demonstrates chloromas as T1-isointense to hypointense, T2-isointense to hypointense (or hyperintense), and markedly enhancing.

Lymphoma (Hodgkin and non-Hodgkin forms) may be focal, multifocal, or diffuse and may have imaging patterns similar to those of other round cell tumors (see Chapter 10). PET-CT is especially helpful for the initial and follow-up evaluations of lymphomas.

Rhabdomyosarcoma, one of the most common solid tumors of childhood, frequently occurs in the first decade (see Chapter 10). This tumor may involve the paraspinal soft tissues or spinal column as a mass, or may represent lymphatic or hematogenous metastasis to the bone marrow. PF/CR, CT, and MRI findings are similar to those for other round cell tumors.

Ewing sarcoma arises from the primitive reticulum stem cell (bone marrow origin) and is a common tumor of childhood. It most often occurs in the second decade as either a primary bone lesion or an extraosseous soft tissue mass with round cell infiltration. PF/CR or CT may show permeative lytic bone destruction. MRI demonstrates additional T1 hypointensity, T2 hypointensity or hyperintensity, and enhancement, especially on fat-suppression images.

Juvenile fibromatosis, an infiltrating process characterized by fibroelastic proliferation, may be focal or diffuse. A congenital form is diffuse with visceral and bone lesions. The juvenile form usually involves the musculoskeletal system. MRI shows a soft tissue mass or masses (T1-isointense to hypointense, T2-isointense to hypointense or hyperintense, with gadolinium enhancement, with use of fat-suppression techniques), that extends along tissue planes and may have bony involvement.

Other "Malignant" Tumors of Mesenchymal Origin

Osteosarcoma is an osteoid-forming neoplasm and the most common primary bone neoplasm of childhood. Subtypes include osteoblastic, chondroblastic, telangiectatic, and fibroblastic. Spinal involvement is infrequent and may be metastatic. In some cases it may be radiation-induced or may arise from an existing lesion (e.g., osteochondroma). PF/CR or CT may show a lytic, sclerotic, or mixed lesion. On MRI, intensity characteristics and enhancement vary according to the extent of tumor ossification. Treatment includes surgery, chemotherapy, and radiotherapy.

Chondrosarcoma is a bone neoplasm of cartilage origin that may originate from an existing lesion (e.g., osteochondroma). PF/CR or CT may show lytic involvement with calcific rings or nodules. MRI may additionally show a heterogenous pattern of T1 and T2 intensities and enhancement.

Chordomas arise from notochordal remnants and are most commonly found in the clivus and sacrum. They are uncommon in childhood. PF/CR or CT shows a lytic lesion with calcification and soft tissue mass. MRI demonstrates additional T1 isointensity or hypointensity, T2 hyperintensity, and enhancement, particularly with use of fat suppression techniques. Treatment includes surgery and radiotherapy.

Tumors of Neural Crest Origin

The spinal tumors of neural crest origin include neuroblastoma, ganglioneuroblastoma, ganglioneuroma, nerve sheath tumors, meningeal tumors, and PNETs. The first three tumors in the

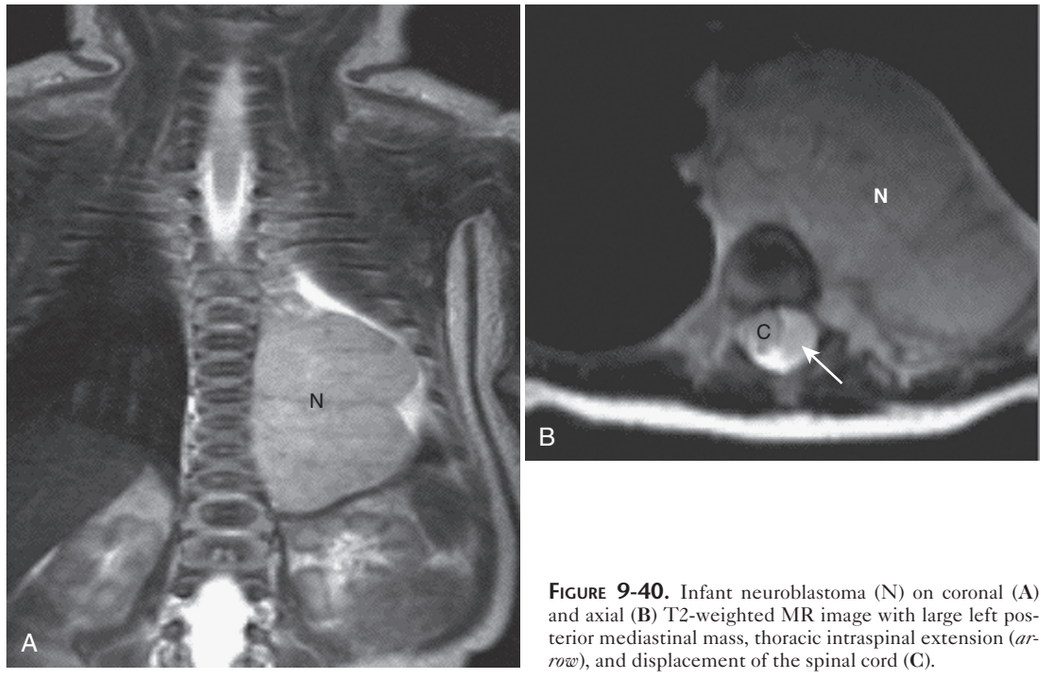

FIGURE 9-40. Infant neuroblastoma (N) on coronal (**A**) and axial (**B**) T2-weighted MR image with large left posterior mediastinal mass, thoracic intraspinal extension (*arrow*), and displacement of the spinal cord (**C**).

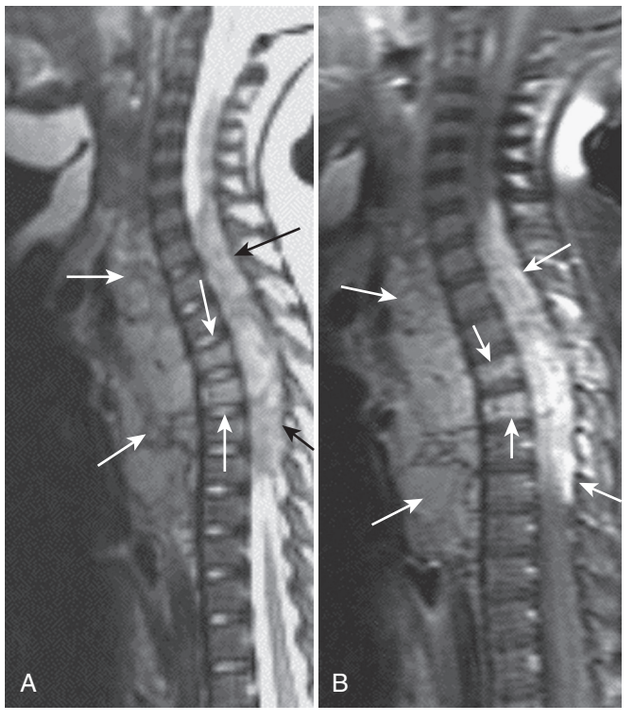

FIGURE 9-41. Thoracic neuroblastoma on sagittal T2-weighted MR image (**A**) and gadolinium-enhanced T1-weighted MR image with fat suppression (**B**). Images show a T2-weighted hyperintense and enhancing posterior mediastinal and paraspinal mass (*anterior long arrows*), intraspinal extension (*posterior long arrows*), and marrow involvement (*vertical arrows*).

previous sentence are listed, and discussed here, in order from "malignant to benign."

Neuroblastoma is the most common solid, non-CNS tumor of childhood (Figs. 9-40 and 9-41). It is composed of neuroblasts and arises within the sympathetic nervous system (e.g., paraspinal sympathetic chain, adrenal medulla, carotid body, aortic bodies, organ of Zuckerkandl). Hematogenous or lymphatic metastases to the spinal marrow often occur. Epidural and transforaminal extension may lead to cord compression. PF/CR or CT may show paraspinal masses with calcification and bony destruction. MRI may show additional T1 isointensity or hypointensity, T2 isointensity, hypointensity, or hyperintensity, and gadolinium enhancement, especially with use of fat suppression. Non-uniform intensities may be related to calcification, hemorrhage, edema, and necrosis. RI is also important because neuroblastoma tends to be avid in uptake of MIBG (iodine-131-meta-iodobenzylguanidine). Neuroblastoma may mature to one of the more benign forms.

Ganglioneuroblastoma is intermediate in malignancy. It contains both mature ganglion cells and immature neuroblast cells. Its behavior may be similar to that of neuroblastoma, including metastases and spinal canal extension.

Ganglioneuroma is a benign tumor consisting of mature ganglion cells. It commonly originates in the posterior mediastinum as a paraspinal mass. PF/CR, CT, or MRI may show a paraspinal mass that is often calcified and enhances. There may be foraminal and intraspinal extension with widening.

Nerve sheath tumors include plexiform neurofibroma (i.e., NF-1; Fig 9-42; see Fig. 9-19), neurofibroma, schwannoma, and malignant nerve sheath tumors. PNETs are rare, extra-CNS neoplasms of primitive neuroepithelial origin. Imaging findings are similar to those for other round cell tumors, including soft tissue mass, bone destruction, and calcification (as discussed earlier).

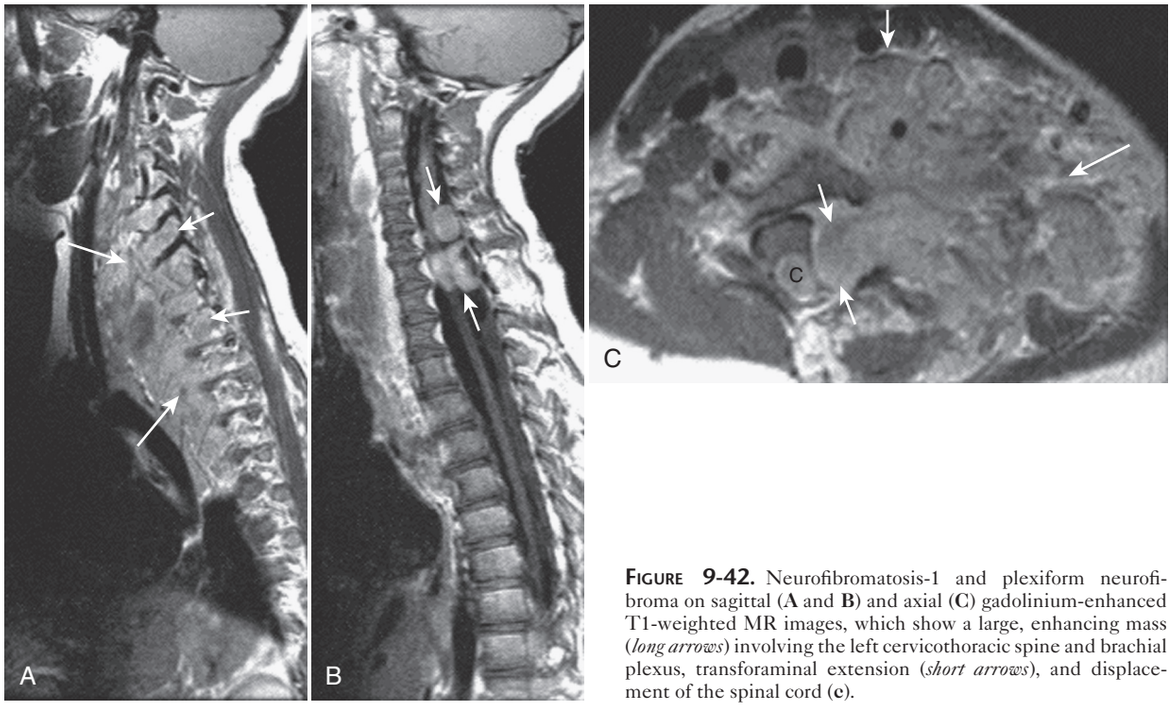

FIGURE 9-42. Neurofibromatosis-1 and plexiform neurofibroma on sagittal (**A** and **B**) and axial (**C**) gadolinium-enhanced T1-weighted MR images, which show a large, enhancing mass (*long arrows*) involving the left cervicothoracic spine and brachial plexus, transforaminal extension (*short arrows*), and displacement of the spinal cord (**c**).

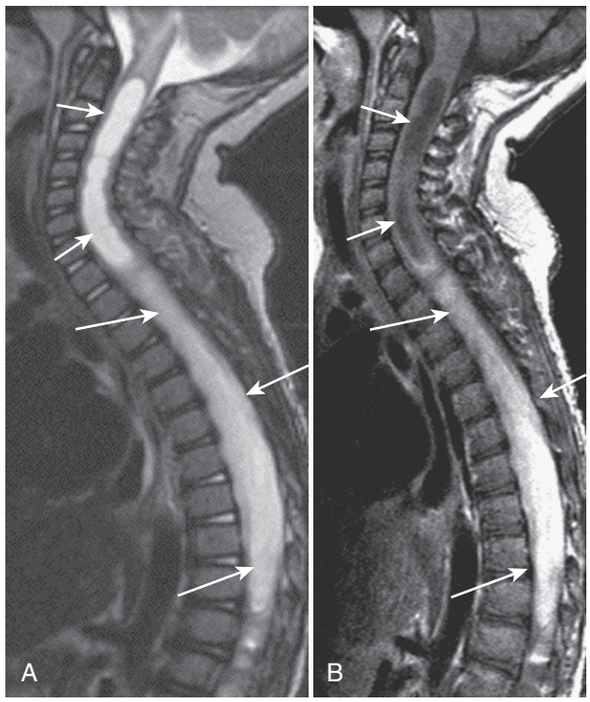

FIGURE 9-43. Cervicothoracic spinal cord astrocytoma on sagittal T2-weighted (**A**) and gadolinium-enhanced T1-weighted (**B**) MR images, which show a T2-hyperintense, enhancing tumor (*long arrows*) with a nonenhancing cystic component (*short arrows*).

Spinal Column Metastases

Metastases to the spinal column are rare in childhood but may occur with rhabdomyosarcoma, neuroblastoma, leukemia, lymphoma, histiocytosis, osteosarcoma, Ewing sarcoma, Wilms tumor, PNET, medulloblastoma, or retinoblastoma. PF/CR or CT may show focal lytic or sclerotic bone destruction (e.g., pathologic fracture), which may be associated with a paraspinal or epidural mass. There may be diffuse homogenous or inhomogeneous marrow involvement. Bone scan (e.g., SPECT) may also detect lesions, but MIBG scanning, PET-CT, or MRI may be more sensitive and specific, depending on the tumor type. MRI intensity and enhancement characteristics of spinal column metastases are similar to those described for round cell tumors.

Intradural (Extramedullary) Tumors

Intradural tumors arise within the dural sac and outside the spinal cord. This category includes tumors of nerve roots and nerve root sheaths (e.g., schwannomas, neurofibromas), neoplastic seeding, developmental tumors (discussed earlier), and meningeal tumors (rare in childhood). Schwannomas often occur sporadically in childhood. MRI shows a mass that is T1-isointense to hypointense and T2-hyperintense, with marked enhancement. Schwannomas and neurofibromas are also frequently associated with the neurofibromatoses (NF-1 or NF-2). Neurofibromas and plexiform neurofibromas consist of Schwann cells and fibroblasts and commonly occur in NF-1. Neurofibrosarcoma or malignant nerve sheath tumor may rarely occur. Extradural paraspinal and spinal involvement is common, including epidural foraminal and intraspinal extension or intradural origin (see Figs. 9-19 and 9-42). MRI shows T1 isointensity or hypointensity, T2 hyperintensity, and enhancement. A heterogenous appearance (e.g., target sign) is characteristic of plexiform neurofibroma. Spinal cord neoplasms are rare in NF-1 (e.g., astrocytoma). NF-2, which occurs more often in adolescence and adulthood, is associated with multiple spinal schwannomas, spinal cord ependymomas, and meningiomas.

Neoplastic seeding of the CSF in childhood occurs most commonly with medulloblastoma (see Chapter 8). Additional sources include other embryonal tumors (e.g., PNET, atypical teratoid rhabdoid tumor, pineoblastoma), germ cell tumors, ependymoma, and malignant glioma. Seeding may rarely occur with astrocytoma, choroid plexus tumors, lymphoma, leukemia, retinoblastoma, or rhabdomyosarcoma. MRI with gadolinium, the imaging modality of choice, may show single or multiple nodules, diffuse or patchy laminar deposits, irregular nerve root thickening or clumping, or subarachnoid space enhancement (see Chapter 8). Hemorrhagic or enhancing postoperative subdural or subarachnoid collections, and inflammatory or infectious processes may mimic neoplastic seeding.

Intramedullary Tumors

Intramedullary tumors arise within the spinal cord. The majority of the intramedullary tumors in childhood are astrocytomas and gangliogliomas, and fewer are ependymomas. Common presenting symptoms include pain, weakness, and scoliosis. MRI shows spinal cord expansion with T1 hypointensity and T2 isointensity and hyperintensity (Fig. 9-43). There may be associated edema, cysts, necrotic cavitation, or hydrosyringomyelia. The tumor often shows nodular or laminar gadolinium enhancement. Astrocytomas are often of low grade and may be circumscribed or infiltrating. Gangliogliomas and ependymomas are often more circumscribed. In childhood, ependymoma more commonly arises along the filum. It may be circumscribed or may infiltrate the conus medullaris and cauda equina nerve roots. Hemorrhage, hemosiderosis, or tumor seeding also occurs with ependymoma. Rarer intramedullary lesions of childhood include mixed gliomas, glioblastoma, PNET, hemangioblastoma (von Hippel–Lindau disease), and metastases (e.g., medulloblastoma via central canal).

Suggested Readings

Ball W Jr: Pediatric Neuroradiology. Philadelphia, Lippincott-Raven, 1997.
Barkovich A: Pediatric Neuroimaging, ed 4. Philadelphia, Lippincott-Raven, 2005.
Blaser SI, Illner A, Castillo M, et al: Peds Neuro: 100 Top Diagnoses. (Pocket Radiologist.) Philadelphia, WB Saunders, 2003.
Harwood-Nash D, Fitz CR: Neuroradiology in Infants and Children. St. Louis, Mosby-Year Book, 1976.
Kirks DR: Practical Pediatric Imaging, ed 3. Philadelphia, Lippincott-Raven, 1998.
Kuhn JP, Slovis TL, Caffey J, Haller JO: Caffey's Pediatric Diagnostic Imaging. ed 10. New York, Elsevier Mosby Saunders, 2003.
Swischuk ME: Imaging of the Newborn, Infant, & Young Child, ed 5. Philadelphia, Lippincott Williams & Wilkins, 2003.
Tortori-Donati P, Rossi A: Pediatric Neuroradiology. New York, Springer, 2005.
van der Knaap MS, Valk J: Magnetic Resonance of Myelination and Myelin Disorders, ed 3. New York, Springer, 2005.
Volpe JJ: Neurology of the Newborn, ed 4. Philadelphia, WB Saunders, 2001.
Wolpert S, Barnes P: MRI in Pediatric Neuroradiology. St. Louis, Mosby-Year Book, 1992.
Zimmerman RA, Gibby WA, Carmody RF (eds): Neuroimaging: Clinical and Physical Principles, New York, Springer, 2000.

Articles and Monographs

Barkovich AJ, Naidich TP (eds): Pediatric Neuroradiology. Neuroimaging Clin North Am 1994;4(2).
Barnes PD (ed): Imaging of the Developing Brain. Top Magn Reson Imag 2007;18(1).
Edwards-Brown MK, Barnes PD (eds): Pediatric Neuroradiology. Neuroimaging Clin North Am 1999;9(1).
Mukherjee P (ed): Advanced Pediatric Imaging. Neuroimaging Clin North Am 2006;16(1).
Mukherji SK (ed): Pediatric Head and Neck Imaging. Neuroimaging Clin North Am 2000;10(1).